Supplemental Materials and Methods

Image quantification

For brain size measurements, all brain samples were isolated from age-matched animals grown side-by-side, and brains were prepared and imaged side-by-side using the same magnification. 2-dimensional projections of each brain were created, and the Zen histogram tool was used to measure the total area of the brain lobes (measured in μm^2) for at least three representative brains for each genotype. Mutant values were normalized to wild-type.

For counting neuroblasts or cortex glia in the central brain, brains from age-matched animals were stained for Dpn to visualize neuroblasts and for SoxN or Repo to visualize cortex glia. Cells were imaged in whole mount brains as 1-2 μm sections at 40x magnification, and images were collected in z-stacks of 2-60 serial optical sections. Dpn-positive nuclei (for neuroblasts), SoxN or Repo positive nuclei (for cortex glia), or Phospho-Histone H3 nuclei in the central brain were counted by hand in each z-stack. Nuclei were counted in at least three brains for each genotype for each experiment. Central brain location of neuroblasts or cortex glia was determined according to cell position in identifiable brain regions and anatomical structures (eg. neuropil, optic lobe neuroepithelial cells).

For quantifying EdU labeling, EdU positive cells were imaged in whole mount brains as 1 μm sections at 40x magnification in serial optical sections collected as z-stacks. The Zen histogram tool was used to measure the total number of pixels for the EdU label in the central brain for each sample. EdU labeling was quantified in at least three representative brains for each genotype for each experiment.

For quantifying cortex glial cell membranes associated with neuroblasts in the central brain, 1500-3000 micron areas in the superficial dorsal central brain (starting typically 4-5 μm below the initial brain surface) were selected in Zen, and the Zen histogram tool was used to compute mean GFP or RFP fluorescence intensities. This technique was adapted from Speder and Brand (2018). All images of matched wild-type controls and mutants were collected with the same laser and gain settings. Mean intensity readings were taken from 3-5 brains per genotype and average intensities for five 1 μm consecutive optical slices were calculated and graphed. Data was normalized to mean fluorescence intensities for the first slice from wild-type controls, and the intensities for all genotypes were graphed per slice relative to each other.

RNA sequencing and human tumor genomics

Primary glioblastoma (GBM) neurosphere cultures were isolated from surgical specimens donated for research with informed consent from patients and were collected and used according to recognized ethical guidelines in a protocol (IRB00045732) approved by the Institutional Review Board at Emory University. GBM cultures were established as per published protocols (Nakano and Kornblum, 2009, Read et al 2013). Normal human neural progenitor cells (HNPCs) were obtained commercially from Lonza. Cell cultures were maintained as neurospheres in DMEM:F12 (Invitrogen) supplemented with 1xB27 (Invitrogen), 50 ng/mL EGF, 20 ng/mL bFGF (R&D Systems), 5 ug/mL heparin (Sigma), and 1x pen/strep as previously described (Read et al., 2013). GBM and HNPC primary cultures were subject to genetic characterization by qPCR for known gene expression alterations commonly found in GBM (EGFR, MET, PDGFR). RNAseq

was performed for each culture as per standard commercial procedures (Beckman Coulter) in which high quality total RNA was isolated from 2-4 million cells from each culture, subject to removal of rRNA and library preparation for next generation sequencing. Primary sequencing data (BAM files) was examined for quality and subject to bioinformatic processing (Winship Bioinformatics Core), assembly, and gene and transcript expression analysis using TopHat and Cufflinks (Trapnell et al., 2012).

mRNA expression data for primary glioblastoma tumor tissue specimens and for lower grade glioma tumor tissue specimens (grade II and III gliomas) was obtained from TCGA datasets through the cBio Portal (www.cbioportal.org) (Brennan et al., 2013; Cancer Genome Atlas Research et al., 2015). The RNA-sequencing data have been deposited in Gene Expression Omnibus under Accession Number GSE122679.

Complete Genotypes for main figures

Figure 1 Genotypes
(A) *UAS-CD8-GFP/+;repo-Gal4/+*
(B) *R108-Gal4/UAS-CD8-GFP*
(C, D) *UAS-dcr;UAS-CD8-GFP;repo-Gal4* heterozygous for the indicated *UAS-RNAi* construct

Figure 2 Genotypes
(A, C, H, I) *UAS-CD8-GFP/+;repo-Gal4/+ , UAS-CD8-GFP/UAS-Pvr^{RNAi};repo-Gal4 , UAS-dcr;UAS-Pvr^{RNAi}/Pvr^{c02195};repo-Gal4 UAS-CD8-GFP/+ , UAS-Pvr$^{\Delta C}$/Pvr^{c02195};repo-Gal4 UAS-CD8-GFP/+ , Pvf1^{ex3};Pvf2-3-crq-Gal4/Pvf2-3- UAS-Pvr$^{\lambda}$;UAS-CD8-GFP/+*
(B, D-G,K-L) *UAS-CD8-GFP/+;repo-Gal4/+ , UAS-CD8-GFP/UAS-Pvr^{RNAi};repo-Gal4/+*
(J) *UAS-CD8-GFP/+;repo-Gal4/+ , UAS-CD8-GFP/UAS-Pvr^{RNAi};repo-Gal4 , UAS-Pvr$^{\Delta C}$/Pvr^{c02195};repo-Gal4 UAS-CD8-GFP/+*

Figure 3 Genotypes
(A, B, C) *UAS-CD8-GFP/+;repo-Gal4/+*
(D) *UAS-CD8-GFP/UAS-Pvr^{RNAi};repo-Gal4*
(E-I) *R122-Gal4 UAS-tdTomato/+ , UAS-dcr;UAS-Pvr^{RNAi}/+;R122-Gal4 UAS-tdTomato/+*

Figure 4 Genotypes
(A) *UAS-CD8-GFP/+;R108-Gal4/+*
(B-F) *Pvf2-lacZ;repo-Gal4 UAS-CD8-GFP/+*

(G-I) from left to right: *UAS-CD8-GFP/+;repo-Gal4/+* , *Pvf1^{ex3};Pvf2-3 crq-Gal4/Pvf2-3 UAS-Pvf2* , *Pvf1^{ex3};Pvf2-3 crq-Gal4 UAS-Pvf2/Pvf2-3 UAS-CD8-GFP;dpn-Gal4/+* , *Pvf1^{ex3};Pvf2-3 crq-Gal4/Pvf2-3 UAS-Pvf2 UAS-CD8-GFP;repo-Gal4/+*
(J) *UAS-CD8-GFP/+;repo-Gal4/+*
(K) *Pvf1^{ex3};Pvf2-3 crq-Gal4/Pvf2-3 UAS-Pvf2;Pax6-EGFP$^{Mi[ET1]MB00408}$*
(L) *Pvf1^{ex3};Pvf2-3 crq-Gal4 UAS-Pvf2/Pvf2-3 UAS-CD8-GFP; dpn-Gal4/+*
(M) *Pvf1^{ex3};Pvf2-3 crq-Gal4/Pvf2-3 UAS-Pvf2 UAS-CD8-GFP;repo-Gal4/+*

Figure 5 Genotypes
(A, B, C) *tGPH/+;R122-Gal4 UAS-tdTomato /+* , *UAS-dcr;tGPH/UAS-Pvr^{RNAi};R122-Gal4 UAS-tdTomato /+*
(C, E, F) *shg-DEcadGFP/+; R122-Gal4 UAS-tdTomato/+* , *shg-DEcadGFP/ UAS-Pvr^{RNAi}; R122-Gal4 UAS-tdTomato/+*
(D) *UAS-CD8-GFP;repo-Gal4/+*, *UAS-Pvr^{RNAi}/+;repo-Gal4 UAS-CD8-GFP/+* , *UAS-dp110^{CAAX}; UAS-Pvr^{RNAi}/+;repo-Gal4 UAS-CD8-GFP/+*, *UAS-Dilp6/UAS-Pvr^{RNAi};repo-Gal4 UAS-CD8-GFP/+*, *UAS-DEcadGFP/UAS-Pvr^{RNAi};repo-Gal4 UAS-CD8-GFP/+*
(G) *UAS-CD8-GFP;repo-Gal4/+*, *UAS-lacZ/UAS-Pvr^{RNAi};repo-Gal4 UAS-CD8-GFP/+* (UAS-lacZ controls for Gal4-UAS gene dose), *UAS-dp110^{CAAX}; UAS-Pvr^{RNAi}/+;repo-Gal4 UAS-CD8-GFP/+*, *UAS-Dilp3/UAS-Pvr^{RNAi};repo-Gal4 UAS-CD8-GFP/+*, *UAS-Dilp6/UAS-Pvr^{RNAi};repo-Gal4 UAS-CD8-GFP/+*, *UAS-DEcadGFP/UAS-Pvr^{RNAi};repo-Gal4 UAS-CD8-GFP/+*
(H, I, K, L) *UAS-CD8-GFP;repo-Gal4/+* , *UAS-lacZ/UAS-Pvr^{RNAi};repo-Gal4 UAS-CD8-GFP/+*, *UAS-DEcadGFP/UAS-Pvr^{RNAi};repo-Gal4 UAS-CD8-GFP/+*

Figure 6 Genotypes
(A-D) *R122-Gal4 UAS-tdTomato/+* , *UAS-Pvf2/+;R122-Gal4 UAS-tdTomato/+* , *UAS-Pvr$^{\lambda}$/+;R122-Gal4 UAS-tdTomato/+*
(E, F) *shg-DEcadGFP/+; R122-Gal4 UAS-tdTomato/+* , *shg-DEcadGFP/UAS-Pvr$^{\lambda}$;R122-Gal4 UAS-tdTomato/+*

Figure 7 Genotypes:
(A-C) *UAS-dEGFR$^{\lambda}$ UAS-dp110^{CAAX}/+;repo-Gal4 UAS-CD8-GFP/+* , *UAS-dEGFR$^{\lambda}$ UAS-dp110^{CAAX}/+;UAS-Pvr^{RNAi}/+;repo-Gal4 UAS-CD8-GFP/+*
(D, E) *UAS-CD8-GFP/+;R122-Gal4/+* , *UAS-dEGFR$^{\lambda}$ UAS-dp110^{CAAX}/+;UAS-CD8-GFP/+;R122-Gal4/+*
(F, G) *shg-DEcadGFP/+; R122-Gal4 UAS-tdTomato/+* , *UAS-dEGFR$^{\lambda}$ UAS-dp110^{CAAX}/+; shg-DEcadGFP/+;R122-Gal4 UAS-tdTomato/+*
(H) *UAS-dEGFR$^{\lambda}$ UAS-dp110^{CAAX}/+;Pvf2-lacZ;repo-Gal4 UAS-CD8-GFP/+*
(I) *UAS-CD8-GFP/+;repo-Gal4/+* , *UAS-dEGFR$^{\lambda}$ UAS-dp110^{CAAX}/+;repo-Gal4 UAS-CD8-GFP/+*

Table S1: An RNAi screen for glial-specific regulators of secondary neurogenesis.

Gene name	RNAi stock IDs	Glia *UAS-dcr;repo-Gal4*	Neuroblasts *UAS-dcr; insc-Gal4 or 2x wor-Gal4*	Neurons *UAS-dcr;elav-Gal4 or ey-Gal4*	Dominant negative, loss-of-function mutants	Flybase and GO pathways, possible function
Akt	v2902, v103703	dramatically decreased larval brain size, little secondary neurogenesis, pupal lethal	semi-lethal in pupae-adults, decreased larval brain size but not as dramatic as glial RNAi		Published roles in fly gliogenesis and neurogenesis (Read et al., 2009; Speder and Brand, 2018)	sole Akt ortholog; PI-3 kinase, RTK-Ras pathways: regulation of cell shape, cell size, differentiation, metabolic process, nervous system development
CG11221	v42947	decreased larval brain size, pupal lethal	grossly normal larval brain size, semi-lethal in pupae and adults			NKF-family kinase; protein metabolic process
CG8485	v35939, v35940	tiny larval brain, little secondary neurogenesis, 3rd instar larval lethal	grossly normal larval brain size	elav-Gal4: larval lethal; ey-Gal4: normal eyes		SNRK-family kinase, act in sugar metabolism process (Ghillebert et al., 2011)
Dsor	v107276	decreased larval brain size, partial reduction neurogenesis, fewer glia, pupal lethal	grossly normal larval brain size, viable adults			sole MEK ortholog; RTK-Ras pathways
EGFR	v43267, v43268, v107130	decreased larval brain size, partial reduction neurogenesis, fewer glia, pupal lethal	no gross larval brain size defects, viable adults			sole EGFR ortholog; PI-3 kinase, RTK-Ras pathways
Gcn2	v103976	tiny brains, little secondary neurogenesis	grossly normal larval brain size, viable adults			sole Gcn2 ortholog: protein metabolism processes, acts as an amino acid sensor (Castilho et al., 2014).
InR	v991, v992	decreased larval brain size, pupal lethal	decreased larval brain size but not as dramatic as glial		Published roles in gliogenesis (Avet-Rochex et al., 2012; Speder and Brand, 2018)	sole IGF1R-Insulin receptor ortholog; PI-3 kinase, RTK-Ras pathways
dp110	v38986	tiny brain, little secondary neurogenesis	decreased larval brain size but not as dramatic as glial, semi-lethal in pupae and adults		Published roles in glial control of neurogenesis (Avet-Rochex et al., 2012; Speder and Brand, 2018)	sole p110 alpha ortholog;PI-3 kinase, RTK-Ras pathways
pitslre	v45127, v107303	tiny brain, little secondary neurogenesis, 3rd instar larval lethal	grossly normal larval brain size, lethal in pupae, no viable adults	grossly normal brains, viable adults		PITSLRE family CDK kinase; regulation of cell shape/cytoskeleton; cell cycle; protein metabolism process
punt	v848	decreased larval brain size, pupal lethal	grossly normal larval brain size, viable adults			ACVR2A/ACVR2B ortholog; BMP/TGF-beta (Dpp) receptor; cell differentiation, nervous system development; protein metabolism processes
Pvr	v105353 v13503	dramatically decreased larval brain size, reduced secondary neurons, pupal lethal, knockdown confirmed by qPCR	grossly normal larval brains with no size reduction, no other defects, viable adults	Elav-Gal4: grossly normal brains with no size reduction, no other defects, viable; ey-Gal4: normal eyes	UAS-PvrΔC dominant negative: reduced brain size; Pvf1-3$^{-/-}$: reduced brain size	PI-3 kinase, RTK-Ras pathways; sole PDGFRA-VEGFR ortholog; RNAi and dominant negative constructs enhanced by Pvr loss-of-function alleles
dRaf	v31038, b31596, v107766	decreased larval brain size, pupal lethal	grossly normal larval brain size, viable adults			sole Raf ortholog; PI-3 kinase, RTK-Ras pathways
sax	v42457 v9434	decreased larval brain size, pupal lethal	grossly normal larval brain size, viable adults			ACVRL1/ACVR1 ortholog; BMP/TGF-beta (Dpp) receptor; differentiation, nervous system development; protein metabolism processes
Tao1	v17432, b35147, v107645	deformed brain: defects in central brain cortex glial morphology, reduced central brain growth, optic lobe overgrowth, pupal lethal	grossly enlarged larval brain size, viable adults			TAO family kinase; Hippo signaling; regulation of cell shape/cytoskeleton; cell cycle; protein metabolism process (Poon et al., 2011)

Table S1: Shown are only those RNAi stocks and corresponding target genes that 1) yielded brain size or neurogenesis phenotypes in the primary screen with *UAS-dcr; repo-Gal4* and that 2) did not show non-specific growth or cell survival phenotypes in neuroblasts and/or neurons as assessed in the secondary screen using the indicated cell-type-specific Gal4 drivers. Note that Tao1 knockdown had a differential effect on brain growth such that the central brain was reduced, but the optic lobe was enlarged, which yielded a statistically insignificant change in total larval brain size (Figure 1D). VDRC stock ID numbers prefaced by "v." Human orthologs were curated from http://kinase.com/

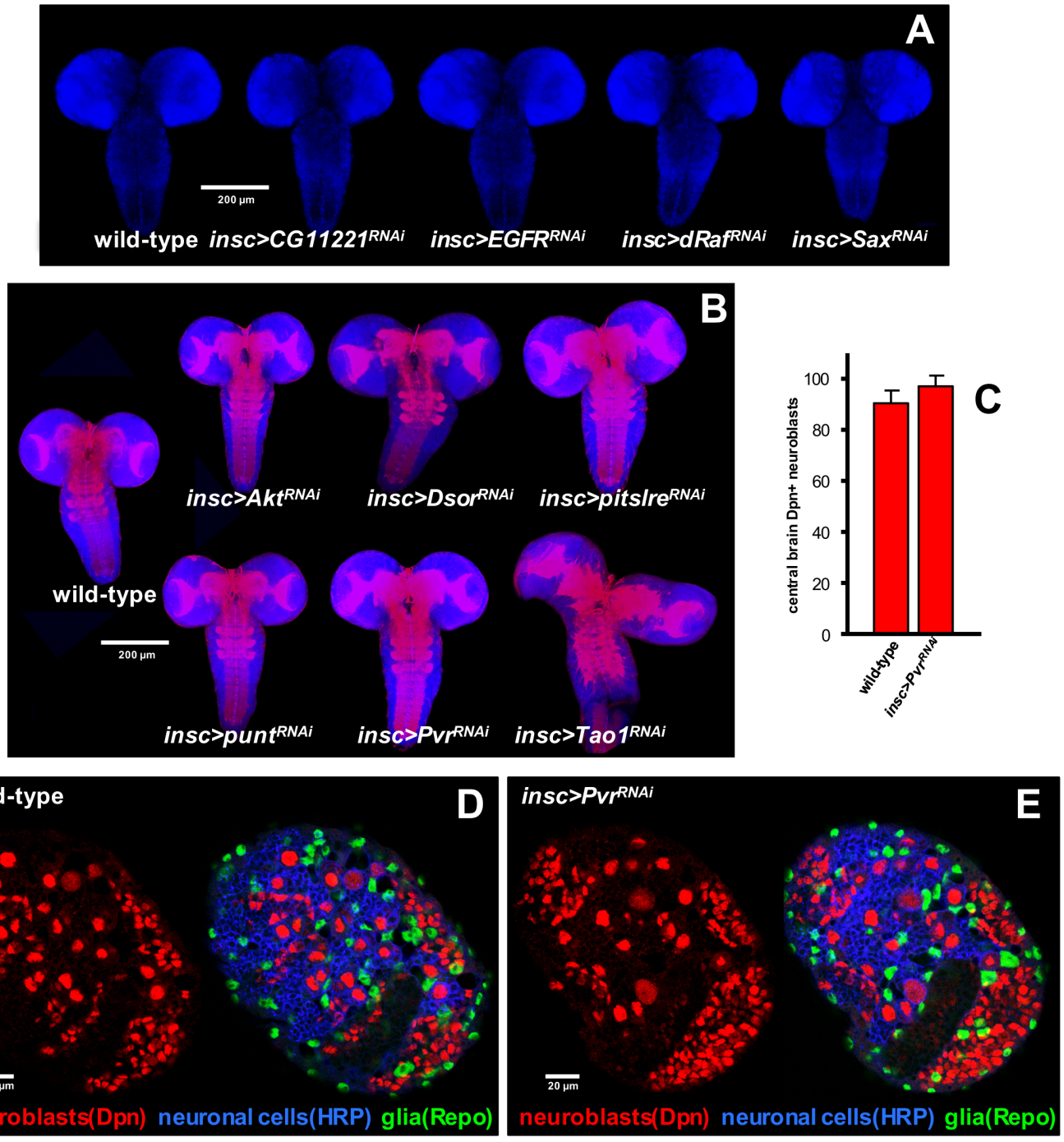

Figure S1: RNAi of candidate genes, including Pvr, in neuroblasts does not yield brain growth phenotypes

(A, B) Late 3rd instar brains, approximately 130 hr AED, at the same scale. Blue labels all cell nuclei and Phalloidin (red) stains actin filaments to visualize brain size. Neuroblast-specific knockdown of indicated genes using *insc-Gal4*.

(C) Neuroblasts (Dpn+) in the central brain counted in 20 µm optical z-stacks of late 3rd instar brain hemispheres of wild-type(n=4) or *insc>Pvr*^{RNAi}(n=4). Values compared with a student's two-

tailed t-test, which showed that expression of a Pvr RNAi construct in neuroblasts is not significantly associated with a reduction in neuroblasts.

(D-E) 2 μm optical sections of representative 3rd instar brain hemispheres. Repo labels glial cell nuclei (green); Dpn-positive labels neuroblasts (red); HRP labels mature and immature neuronal cell bodies (blue). *insc>Pvr*^{RNAi} brains showed no obvious alterations in size and no obvious decrease in glial cells, neuroblasts, or neurons compared to wild-type controls.

Figure S1 Genotypes:
(A) *UAS-dcr/+;insc-Gal4/+* with the indicated *UAS-RNAi* construct
(C-E) *UAS-dcr/+;insc-Gal4/+*, *UAS-dcr/+;insc-Gal4/UAS-Pvr*^{RNAi}

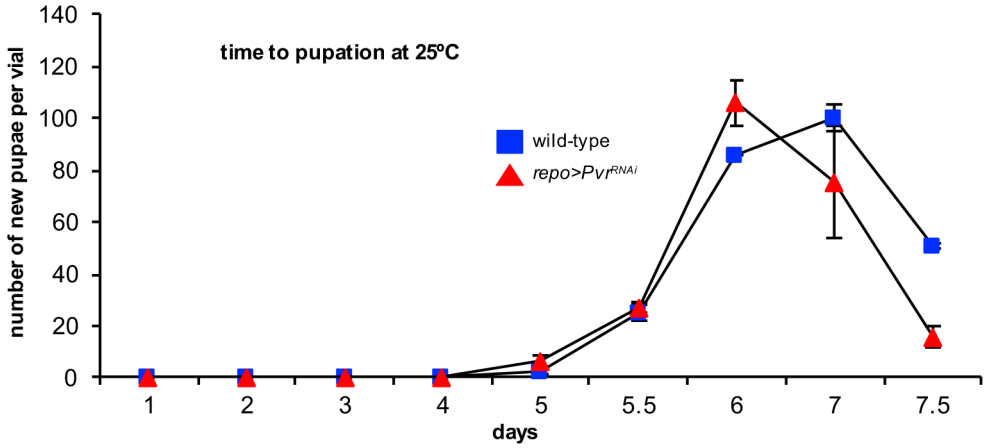

Figure S2: Glial-specific RNAi does not cause gross developmental delays

Embryos of r*epo>CD8-GFP* wild-type or *repo>Pvr*^{RNAi} genotypes were collected from parental crosses (20-25 females each) in vials for 24 hours and reared on standard food, 3 vials for each genotype. Once or twice each day (~12-24 hours) new pupae within each vial were counted. The graph shows the average number of new pupae per vial on the indicated day following embryo collection. Error bars show standard error of the mean. A paired student's t-test showed no statistically significant differences in time to pupation between the two genotypes.

Figure S2 Genotypes:
UAS-CD8-GFP/+;repo-Gal4/+
UAS-Pvr^{RNAi}*/UAS-CD8-GFP;repo-Gal4 /+*

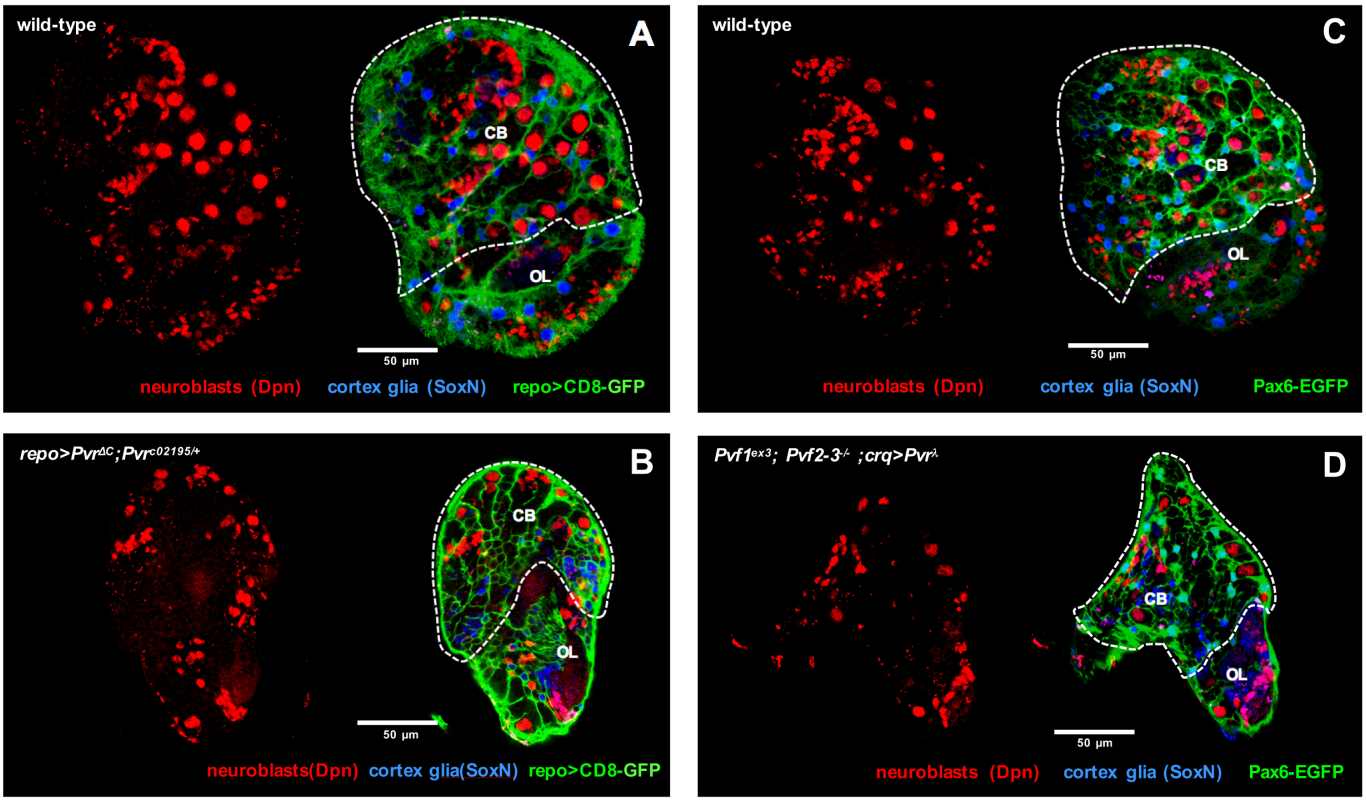

Figure S3: Pvr is required for neuroblast maintenance and cortex glia morphogenesis and survival

(A, B) 2 µm optical sections of age-matched 3rd instar brain hemispheres. Anterior up; midline to left. White dashed lines roughly outline the central brain (CB) relative to the optic lobe (OL). Dpn (red) labels neuroblasts. Strong SoxN staining (blue) labels cortex glial cell nuclei, and weakly labels neuroblasts and ganglion mother cells (GMCs) in the central brain and optic lobe (pink-purple in overlays). (A, C) *repo>CD8-GFP* (green) labels glial cell bodies and processes. (B) *repo>Pvr$^{\Delta C}$; Pvr$^{C02195/+}$* mutant brains showed decreased over-all size, reduced glial processes, and reduced SoxN and Dpn-positive cells in the central brain, as compared to (A) wild-type.

(C, D) 2 µm optical sections of age-matched 3rd instar brain hemispheres. Anterior up; midline to left. White dashed lines roughly outline the central brain (CB) relative to the optic lobe (OL). Dpn (red) labels neuroblasts. Strong SoxN staining (blue) labels cortex glial cell nuclei, and weakly labels Dpn-positive neuroblasts and intermediate neuronal progenitor cells in the central brain and optic lobe (pink-purple in overlay). Pax6-EGFP (green) labels cortex glial cell bodies and processes (Metaxakis et al., 2005). (B) *Pvf1^{ex3}; Pvf2-3$^{-/-}$ crq>Pvr$^{\lambda}$* mutant brains showed decreased over-all size, reduced glial processes, and reduced SoxN and Dpn-positive cells in the central brain, as compared to (A) wild-type.

Figure S3 Genotypes:
(A) *UAS-CD8-GFP/+;repo-Gal4/+*
(B) *UAS-Pvr$^{\Delta C}$/Pvr^{C02195};repo-Gal4 UAS-CD8-GFP/+*
(C) *Pax6-EGFP$^{Mi[ET1]MB00408}$*
(D) *Pvf1^{ex3};Pvf2-3$^{-/-}$ crq-Gal4/Pvf2-3^{-} UAS-Pvr$^{\lambda}$;Pax6-EGFP$^{Mi[ET1]MB00408}$*

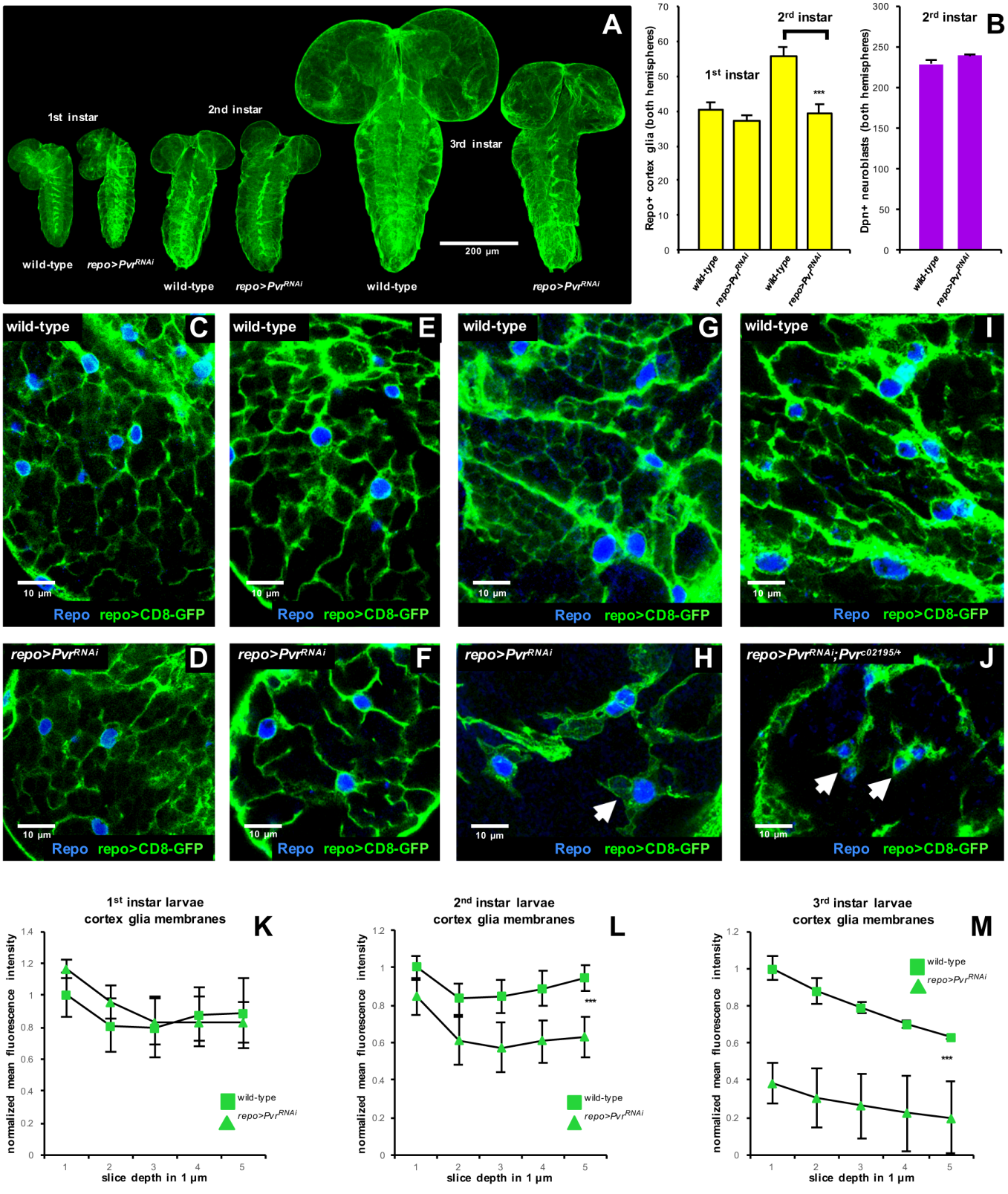

Figure S4: Pvr is required for cortex glia morphogenesis and survival

(A) Optical projections of age-matched whole brain-ventral nerve cord complexes; same scale. Dorsal view; anterior up. Glial cell bodies labeled by membrane-bound CD8-GFP driven by *repo-Gal4*.

(B) Neuroblasts (Dpn+) in the central brain counted in confocal z-stacks of whole 2nd instar brains: wild-type(n=3), *repo>Pvr*^{RNAi}(n=3). Cortex glia (Repo+) in the central brain counted in confocal z-stacks of whole 1st and 2nd instar brains: wild-type(n=4, n=4), *repo>Pvr*^{RNAi}(n=4, n=4). Values for each mutant compared to wild-type by student's two-tailed t-test, which showed that loss of Pvr signaling caused a statistically significant loss of cortex glia, but not of neuroblasts, in 2nd instar larvae relative to wild-type; ***p-$value$ <.005.

(C-J) Close-ups of 1-2 μm optical sections to show cortex glia morphology in age-matched (C, D) 1st instar, (E, F) early 2nd instar, and (G, H) early 3rd instar (brains shown at the same scale. *repo>CD8-GFP* (green) labels glial cell bodies; Repo (blue) labels all glial nuclei. In wild-type, (C) 1st instar cortex glia show processes that partially wrap neighboring neuronal cells. In wild-type, (E, G, I) 2nd and 3rd instar cortex glia develop thick and fine processes, which extensively wrap the cell bodies of neurons and their progenitors to form honeycomb patterns throughout the brain. In 1st instar, (D) *repo>Pvr*^{RNAi} animals show cortex glia with processes comparable to those of wild-type controls, but by 2nd instar (F) cortex glia in *repo>Pvr*^{RNAi} show reduced processes relative to wild-type controls, and in 3rd instar *repo>Pvr*^{RNAi} and *repo>Pvr*^{RNAi}*; Pvr*$^{c02195/+}$ animals (H, J) cortex glia showed dramatically reduced processes, small cell bodies, and pyknotic, faint nuclei (arrows).

(K-M) Cell membrane fluorescence intensities of cortex glia in the central brain, normalized to wild-type control values, plotted over a 5 μm depth. Mean intensities are not significantly different between wild-type (n=4, each stage) and *repo>Pvr*^{RNAi}(n=4, each stage) at 1st instar, but are significantly different in 2nd and 3rd instar stages. Values for *Pvr*^{RNAi} compared to wild-type with paired student's t-tests; ***p-$value$ <.005.

Figure S4 Genotypes:
(A, B, C, E, G, I, K-M) *UAS-CD8-GFP/+;repo-Gal4/+*
(A, B, D, F, K-M) *UAS-dcr;UAS-Pvr*^{RNAi}*/UAS-CD8-GFP;repo-Gal4/+* (included *UAS-dcr* to potentially enhance phenotypes in 1st and 2nd instar larvae)
(A, H) *UAS-Pvr*^{RNAi}*/UAS-CD8-GFP;repo-Gal4 /+* (3rd instar larvae)
(J) *Pvr*$^{c02195/+}$*/UAS-Pvr*^{RNAi}*;repo-Gal4 UAS-CD8-GFP/+*

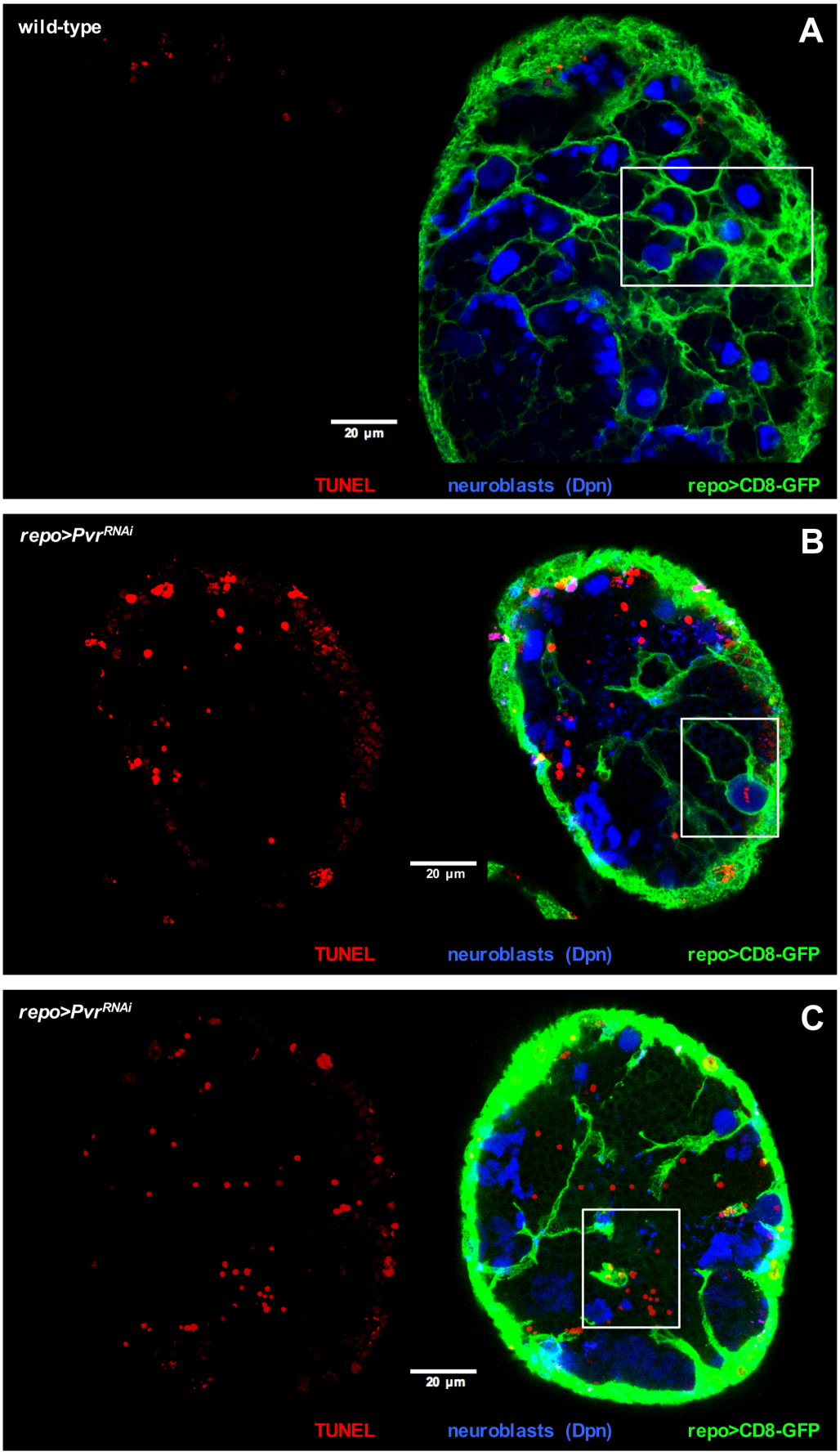

Figure S5: Pvr is required for survival of glia, neuroblasts, and neurons

(A-C) 3 μm optical sections of the central brain in 3rd instar larvae, whole brain hemispheres from which the close-ups in Figure 2 are shown. *repo>CD8-GFP* labels glia; Dpn (blue) labels neuroblast nuclei; red labels TUNEL+ cells in wild-type and *repo>Pvr*^{RNAi} (right) brains. TUNEL+ neuroblasts (shown in close-up in Figure 2K) and cortex glia and neurons (shown in close-up in Figure 2L) were present in *repo>Pvr*^{RNAi} brains. TUNEL-positive immature neurons were determined by position and lack of Dpn+ or GFP labeling. (A) wild-type shows a total of 3-4 TUNEL-positive spots, that may be neuronal nuclei.

Figure S5 genotypes:
(A) *UAS-CD8-GFP/+;repo-Gal4/+*
(B, C) *UAS-CD8-GFP/UAS-Pvr*^{RNAi}*;repo-Gal4*

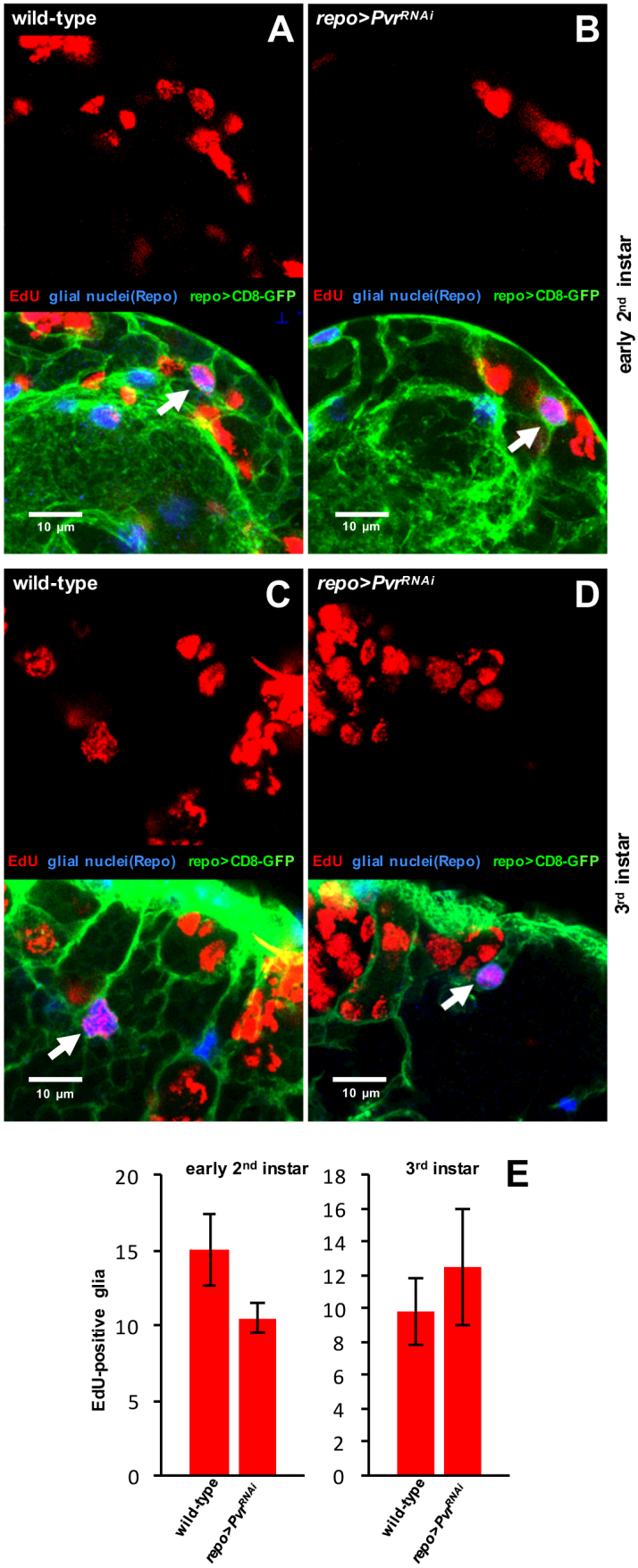

Figure S6: Pvr is not required for cortex glia proliferation

(A-D) Close-ups of 2 μm optical sections to show proliferative cortex glia in (A, B) early 2nd instar brains, at the onset of secondary neurogenesis, and in (C, D) 3rd instar brains. *repo>CD8-GFP* labels glial cells; Repo (blue) labels glial cell nuclei; EdU (red) labels S-phase and M-phase cells. (B, D) *repo>Pvr*^{RNAi} brains showed similar numbers of proliferative cortex glia (white arrows, magenta in overlays show Repo+ EdU+ cortex glial cells) as (A, C) wild-type control brains during early 2nd instar through to 3rd instar during secondary neurogenesis.

(E) EdU-positive glia in the dorsal central brain counted in 36-42 μm optical z-stacks of early 2nd instar and in 46-48 μm optical z-stacks of late 3rd instar brain hemispheres. 2nd instar: wild-type(n=3), *repo>Pvr*^{RNAi}(n=4), 3rd instar: wild-type(n=2), *repo>Pvr*^{RNAi}(n=5). Values for each mutant compared to wild-type with a student's two-tailed t-test, which showed that Pvr RNAi is not significantly associated with reduced EdU-labeling in glia. Bars show standard error of the mean.

Figure 6 Genotypes:
(A, C, E) *UAS-CD8-GFP/+;repo-Gal4/+*
(B, D, E) *UAS-Pvr*^{RNAi}*/UAS-CD8-GFP;repo-Gal4/+*

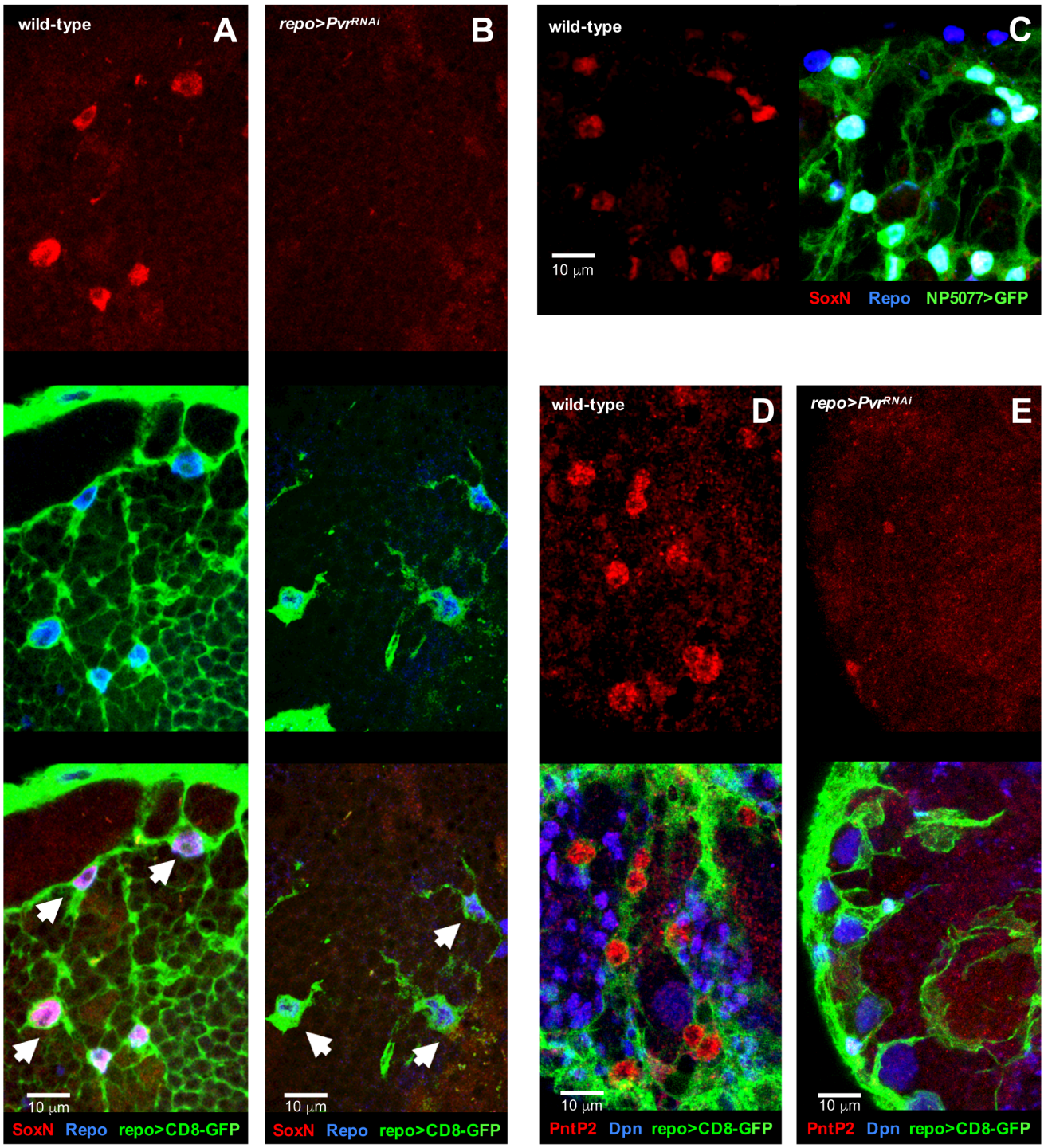

Figure S7: SoxN and PntP2 transcription factors are expressed by cortex glia in the central brain

(A, B) Close-ups of 1-2 μm optical sections to show cortex glia in early 3rd instar brains from (A) wild-type and (B) *repo>Pvr*^{RNAi} at the same scale. *repo>CD8-GFP* (green) labels glial cell bodies; Repo (blue) labels all glial nuclei. The SoxN transcription factor (red) labels cortex glia in the central brain in (A) wild-type (red, purple in overlay), but SoxN was lost in central brain cortex glia with (B) Pvr knockdown (evidenced by no red, no purple in overlay).

(C) Close-up of 2 μm optical sections to show cortex glia in early 3rd instar brains from (A) wild-type. UAS-CD8-GFP expressed by *NP5077-Gal4* (green) specifically labels cortex glia cell bodies (Awasaki et al., 2008); SoxN (red, cyan in overlay) labels cortex glia nuclei in the central brain; Repo (blue) labels all glial nuclei.

(E, F) Close-ups of 1-2 μm optical sections to show cortex glia in early 3rd instar brains from (A) wild-type and (B) *repo>Pvr*^{RNAi} at the same scale. *repo>CD8-GFP* (green) labels glial cell bodies; Dpn (blue) labels neuroblast nuclei. The PntP2 transcription factor (red) labels cortex glia in the central brain in (A) wild-type (red, purple in overlay), but PntP2 was lost in central brain cortex glia with (B) Pvr knockdown (evidenced by no red in overlay).

Figure S7 Genotypes:
(A, E) *UAS-CD8-GFP/+ ; repo-Gal4/+*
(B, F) *UAS-Pvr*^{RNAi}*/+; repo-Gal4 UAS-CD8-GFP/+*
(C) *NP5077-Gal4/UAS-CD8-GFP*

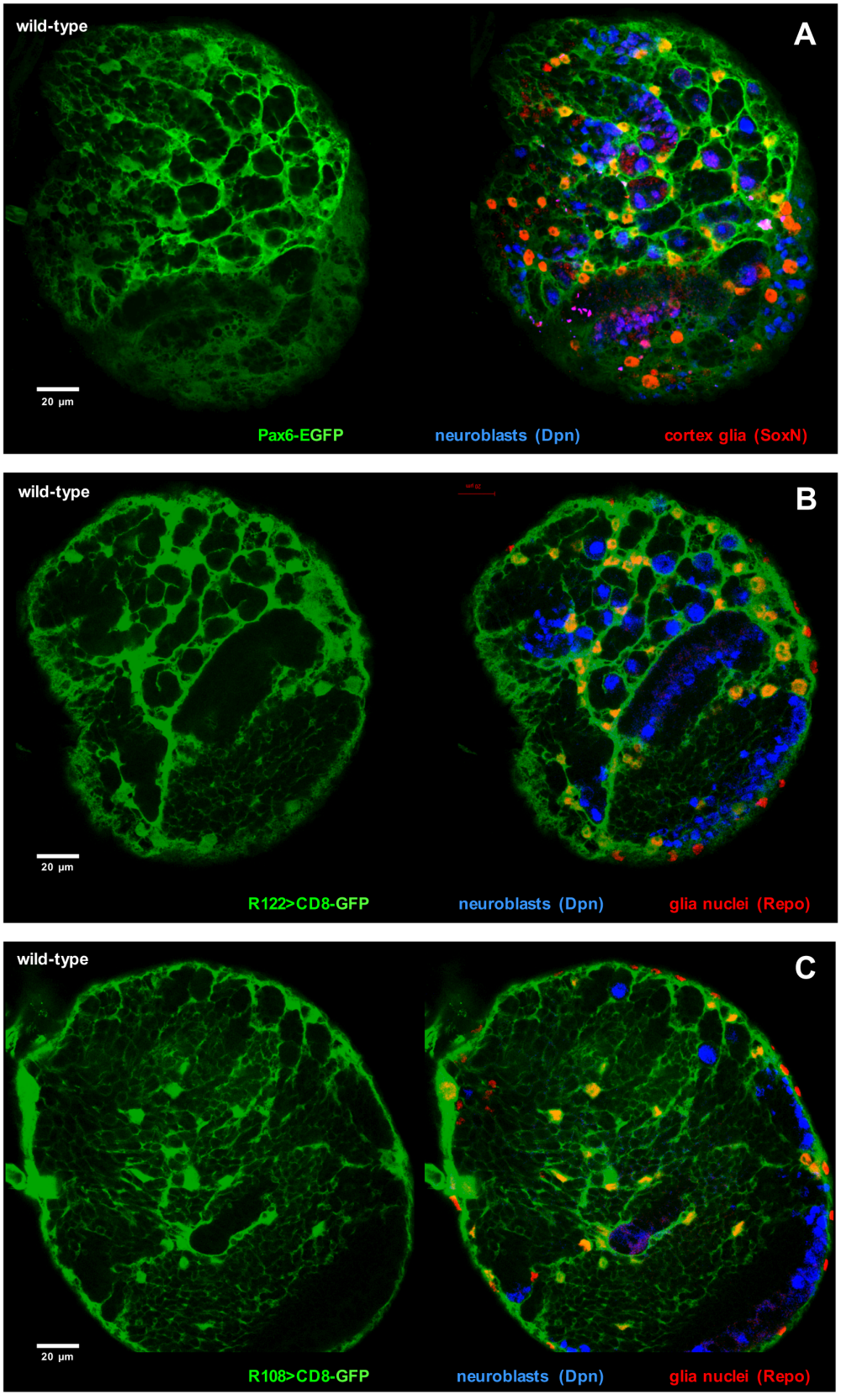

Figure S8: Cortex glia specific markers and drivers

(A) 2 µm optical sections of age-matched 3rd instar brain hemispheres. Anterior up; midline to left. Dpn (blue) labels neuroblasts. Strong SoxN staining (red) labels cortex glial cell nuclei, and

weakly labels Dpn-positive neuroblasts and intermediate neuronal progenitor cells (magenta in overlay). Pax6-EGFP (green) labels cortex glial cell bodies and processes (Metaxakis et al., 2005).

(B, C) 2 μm optical sections to show 3rd instar brain hemispheres from animals that contain a UAS-CD8-GFP transgene driven by Gal4 drivers specific to cortex glia, either (A) *R122-Gal4* or (B) *R108-Gal4*, which were isolated in the lab through a genetic screen for cortex-glial specific drivers. Repo (red) labels glial cell nuclei; Dpn (blue) labels neuroblasts.

Figure S8 Genotypes:
(A) *Pax6-EGFP*$^{Mi[ET1]MB00408}$
(B) *R122-Gal4/UAS-CD8-GFP*
(C) *R108-Gal4/UAS-CD8-GFP*

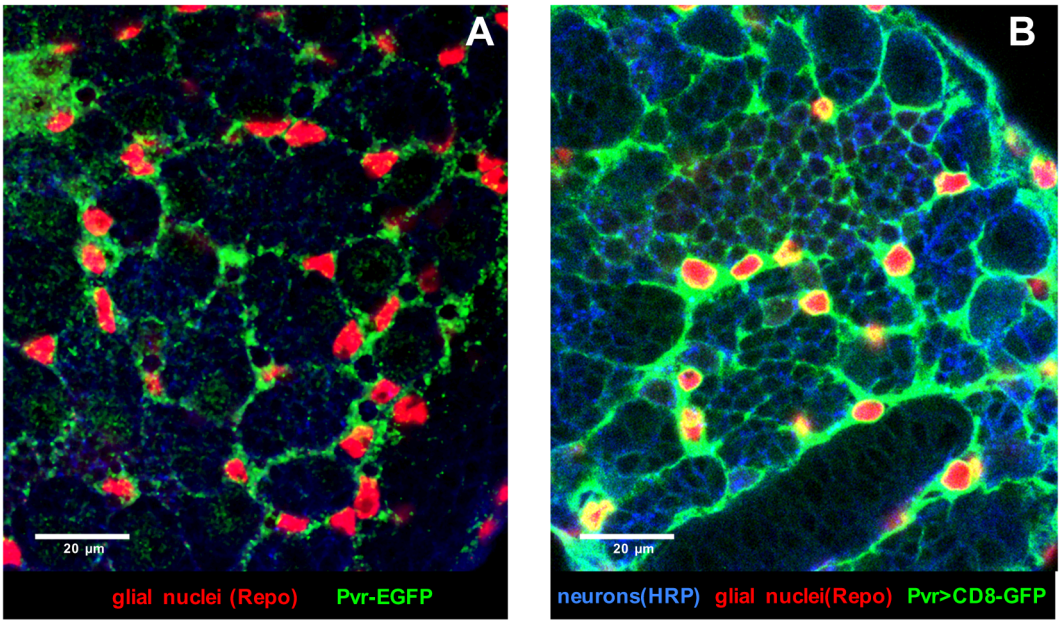

Figure S9: Pvr is expressed in cortex glia

(A) Close-up of 2 µm optical sections to show cortex glia in early 3rd instar brains from (A) animals homozygous for a Pvr-EGFP$^{MI04181\text{-}GFSTF}$ gene trap. Repo (red) labels glial cell nuclei; *Pvr-EGFP* (green) labels cell bodies of all Pvr expressing cells, which are cortex glia in the central brain.

(B) Close-up of 2 µm optical sections to show cortex glia in early 3rd instar brains from (A) animals that contain a UAS-CD8-GFP transgene driven by a Gal4 inserted into the Pvr gene (*Pvr-Gal4*$^{MI04181\text{-}TG4}$). Repo (red) labels glial cell nuclei; HRP (blue) labels neuronal cells; *Pvr>CD8-GFP* (green) labels cell bodies of all Pvr expressing cells, which are cortex glia in the central brain.

Figure S9 Genotypes:
(A) *Pvr-EGFP*$^{MI04181\text{-}GFSTF}$
(B) *Pvr-Gal4*$^{MI04181\text{-}TG4}$*/UAS-CD8-GFP*

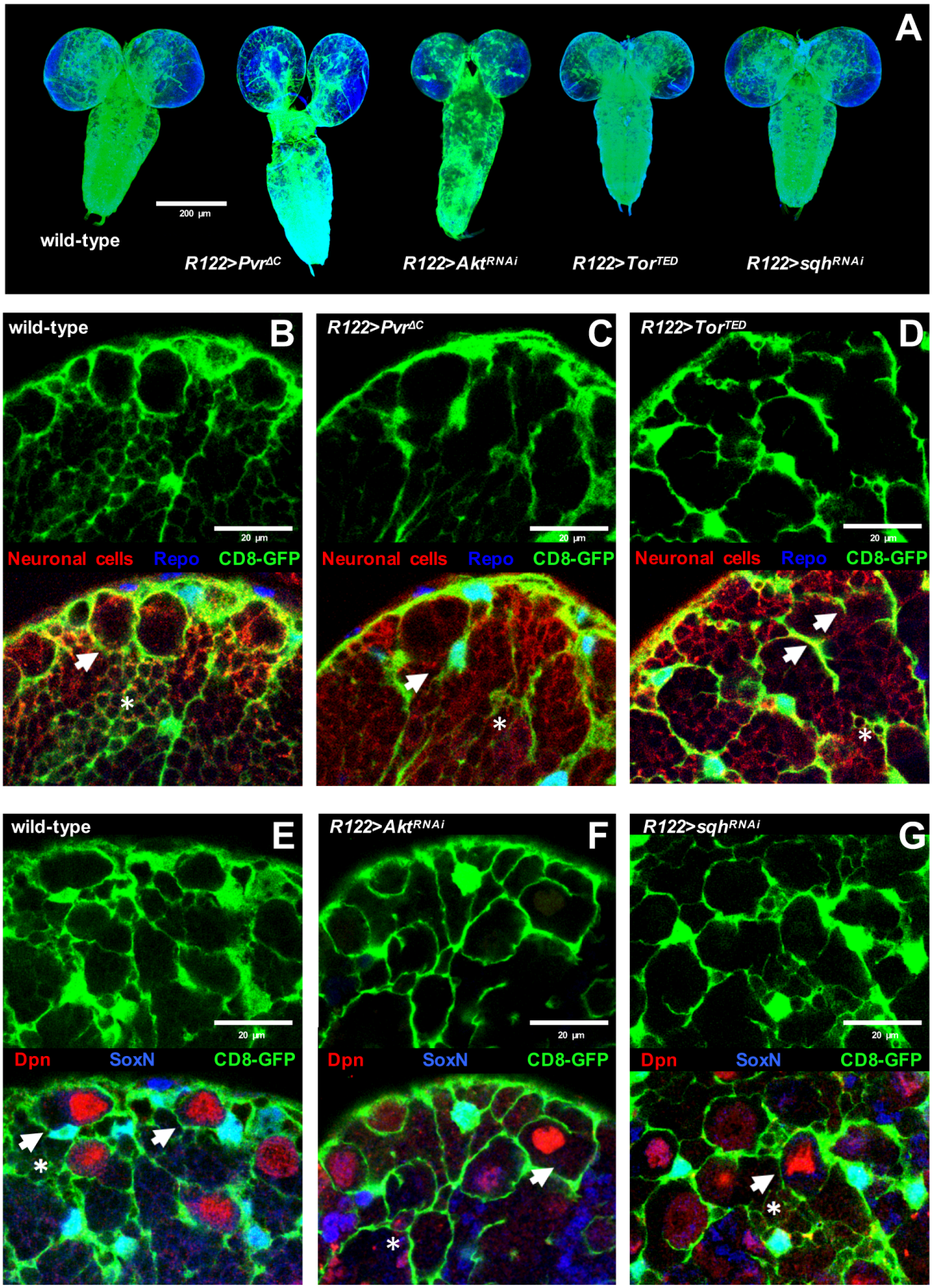

Figure S10: Pvr and PI3K signaling are required in cortex glia for niche morphogenesis and secondary neurogenesis

(A) Late 3rd instar larval brains, approximately 130 hr AED, all at the same scale. Blue shows all cell nuclei (DRAQ7). Dorsal view; anterior up. Transgenes driven by cortex glia specific *R122-*

Gal4. Membrane-associated-RFP (UAS-tdTomato) labels cortex glial cell bodies and processes (tdTom, false-colored green). Brain lobe size is reduced in animals that express dominant negative Pvr ($Pvr^{\Delta C}$), Akt RNAi (Akt^{RNAi}), or dominant negative mTor (Tor^{TED}) in cortex glia. Brain size was unchanged by expression of *sqh* RNAi (sqh^{RNAi}) in cortex glia. *sqh* (*spaghetti squash*) encodes the sole *Drosophila* ortholog of MRLC, which is an effector of Rac-Rho signaling (Van Aelst and Symons, 2002).

(B-G) 1-2 μm optical sections of the central brain in age-matched 3rd instar brains, all at the same scale. Anterior up; midline to left. Transgenes expressed in cortex glia by the *R122-Gal4* driver. R122>tdTom labels cortex glia cell bodies and processes (tdTom, false-colored green). In wild-type (B, E), cortex glia form thick processes encircling neuroblasts (arrows) and their progeny as well as fine processes that wrap neuronal cell bodies to form a honeycomb pattern in deeper brain regions (asterisks). Cortex glia processes are reduced (arrows and asterisks highlight examples) by expression of (C) dominant negative Pvr ($Pvr^{\Delta C}$), (F) Akt RNAi constructs (Akt^{RNAi}), or (D) dominant negative mTor (Tor^{TED}), whereas *sqh* RNAi constructs (sqh^{RNAi}) had a minimal effect (arrow, asterisk). (B, C, D) Repo (blue) labels all glial nuclei; anti-HRP stain (red) shows neuronal cell bodies, including neuroblasts and neurons; (E, F, G) Dpn (red) labels neuroblasts; SoxN strongly labels cortex glia nuclei (blue overlaid with green) and weakly labels neuroblasts (purple with Dpn overlay) and their progeny in the central brain (small faint blue cells).

Figure S10 Genotypes:
(A-G) *R122-Gal4 UAS-tdTomato/+ , UAS-*$Pvr^{\Delta C}$*/+;R122-Gal4 UAS-tdTomato/+ , UAS-dcr/+; UAS-*Akt^{RNAi}*/+; R122-Gal4 UAS-tdTomato/+ , UAS-*Tor^{TED}*/R122-Gal4 UAS-tdTomato/+ , UAS-dcr/+; UAS-*sqh^{RNAi}*/R122-Gal4 UAS-tdTomato*

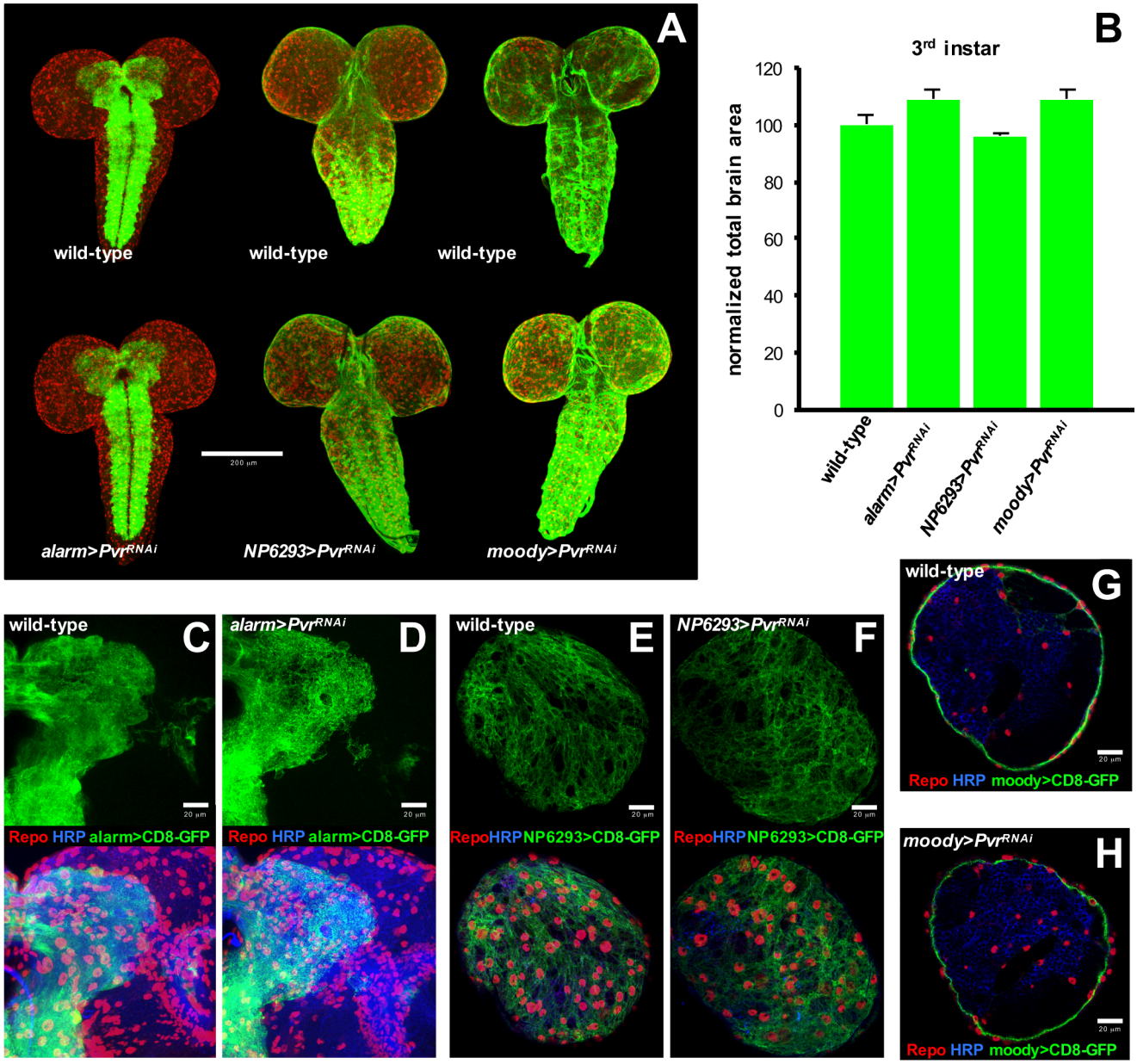

Figure S11: Overexpression of Pvr^{RNAi} in other glial subtypes does not yield larval brain growth defects

(A) Late 3rd instar larval brains, approximately 130 hr AED, all at the same scale. Repo (red) shows all glial cell nuclei. Dorsal view; anterior up. In wild-type brains (upper), membrane-associated-GFP (UAS-CD8-GFP, green) labels astrocytes (*alarm-Gal4*), perineurial glia (*NP6293-Gal4*), and subperineurial glia (*moody-Gal4*) cell bodies and processes. (Lower) brain size was unchanged by expression of Pvr RNAi constructs (*Pvr^{RNAi}*) in astrocytes (*alarm-Gal4*), perineurial glia (*NP6293-Gal4*), or subperineurial glia (*moody-Gal4*).

(B) Brain size calculated using total brain area, measured in µm^2 in optical projections of late 3rd instar brains, normalized to wild-type controls. Values for *alarm>Pvr^{RNAi}*(n=4), *NP6293>Pvr^{RNAi}*(n=4), and *moody>Pvr^{RNAi}*(n=4) compared to wild-type controls (n=4) with student's two-tailed t-tests; none showed statistically significant differences in brain size between Pvr-RNAi and wild-type controls.

(C-H) Late 3rd instar larval brains, approximately 130 hr AED, all at the same scale. Repo (red) shows all glial cell nuclei. Dorsal view; anterior up. Membrane-associated-GFP (UAS-CD8-GFP, green) labels astrocytes (*alarm-Gal4*), perineurial glia (*NP6293-Gal4*), and subperineurial glia (*moody-Gal4*) cell bodies and processes. (C-D) optical projections of 20 µm z-stacks; astrocytes did not show major differences between wild-type and *alarm>Pvr^{RNAi}* brains. (E-F) 2 µm optical projections; perineurial glia showed not major differences between wild-type and *NP6293>Pvr^{RNAi}* brains. (G-H) 2 µm optical projections; subperineurial glia showed not major differences between wild-type and *moody>Pvr^{RNAi}* brains.

Figure S11 Genotypes:
(B) *UAS-CD8-GFP; alarm-Gal4 /+, N6293-Gal4; UAS-CD8-GFP/+, UAS-CD8-GFP; moody-Gal4 /+ , UAS-dcr; UAS-Pvr^{RNAi}/UAS-CD8-GFP; alarm-Gal4 /+, UAS-dcr; UAS-Pvr^{RNAi}/N6293-Gal4; UAS-CD8-GFP/+, UAS-dcr; UAS-Pvr^{RNAi}/UAS-CD8-GFP; moody-Gal4 /+*
(C-H) *UAS-CD8-GFP; alarm-Gal4 /+, UAS-dcr; UAS-Pvr^{RNAi}/UAS-CD8-GFP; alarm-Gal4 /+, N6293-Gal4; UAS-CD8-GFP/+, UAS-dcr; UAS-Pvr^{RNAi}/N6293-Gal4; UAS-CD8-GFP/+, UAS-CD8-GFP; moody-Gal4 /+, UAS-dcr; UAS-Pvr^{RNAi}/UAS-CD8-GFP; moody-Gal4 /+*

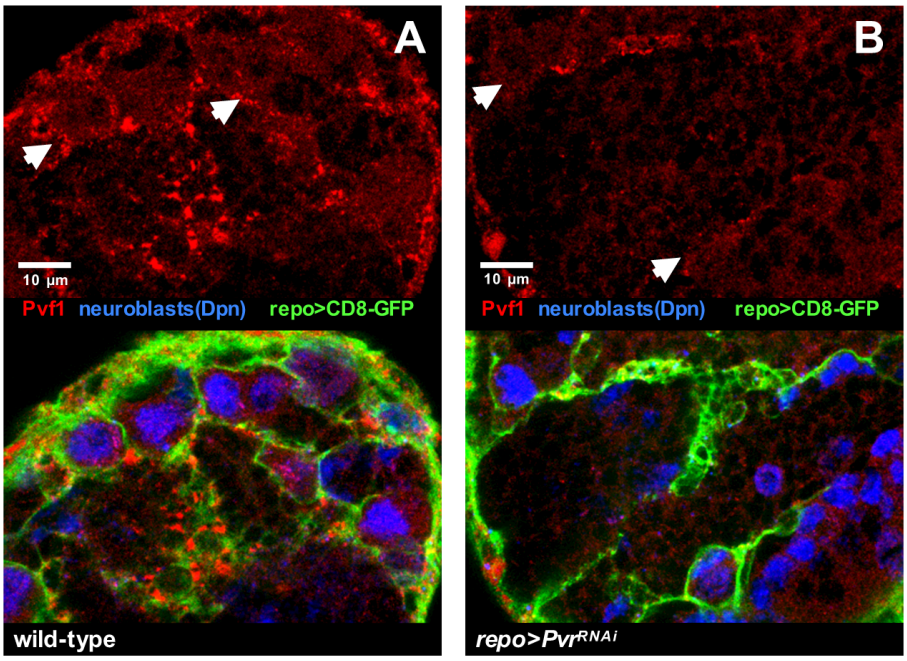

Figure S12: Pvf1 protein associates with cortex glia cell membranes in a Pvr-dependent manner

(A, B) 2 µm optical sections of the central brain of early 3rd instar (A) wild-type larvae or (B) *repo>Pvr*^{RNAi} larvae. (A, B) Glial cell membranes labeled with *repo>CD8-GFP* (green); Dpn (blue) labels neuroblast nuclei. (A) Pvf1 protein (red) is present on cortex glial cell membranes (for examples see arrows). (B) Pvf1 staining on cortex glial cell membranes is reduced by Pvr knockdown.

Figure S12 Genotypes:
(A) *UAS-CD8-GFP/+;repo-Gal4/+*
(B) *UAS-Pvr*^{RNAi}*/+;repo-Gal4 UAS-CD8-GFP/+*

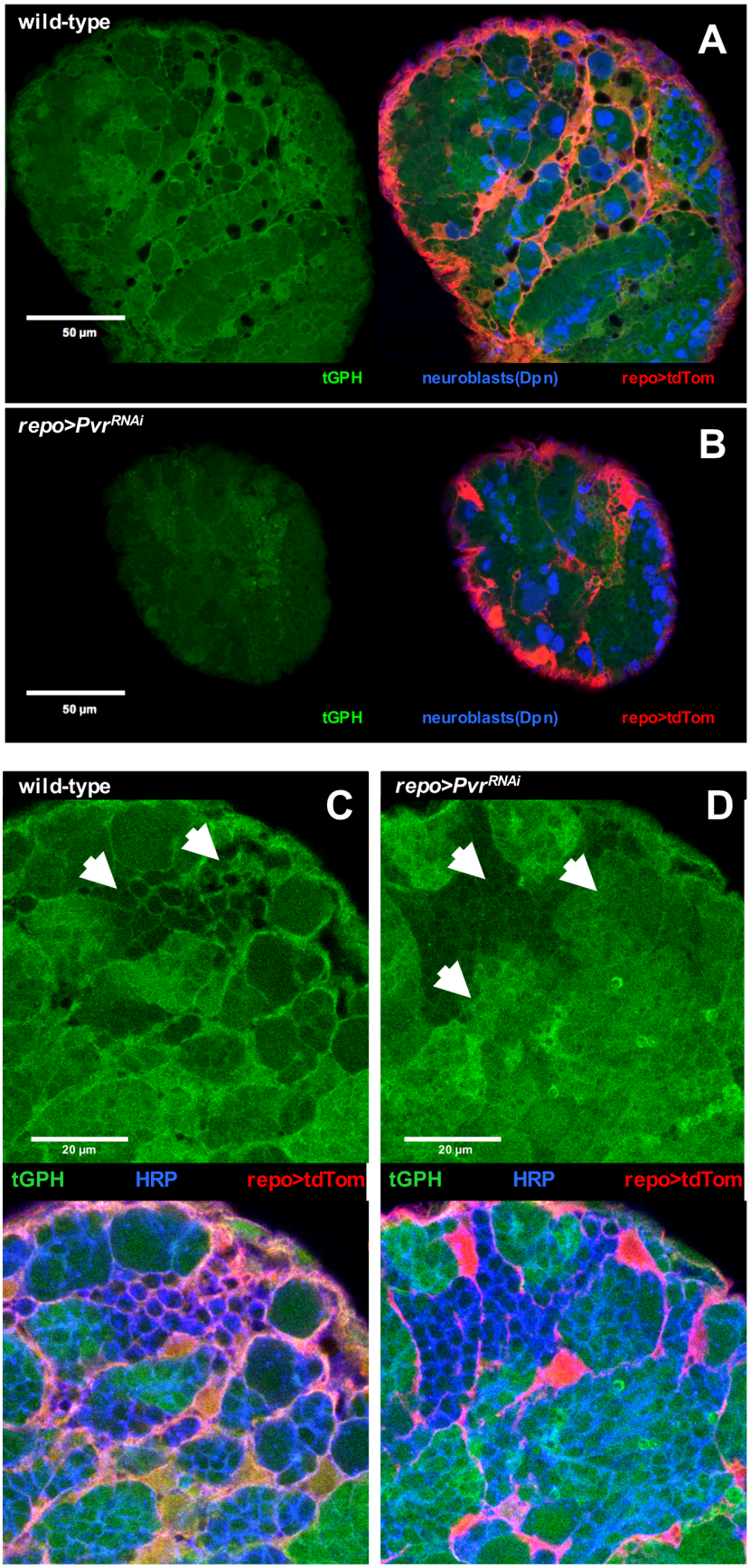

Figure S13: Loss of glial Pvr function causes cell non-autonomous loss of PI3K signaling in neurons

(A-D) 2 μm optical sections of 3rd instar brains, at the same scale. Green shows tGPH reporter localization; *repo>tdTom* (red) labels cortex glia membranes; anti-HRP (blue) labels neuronal cell bodies. (A, C) in wild-type, membrane-associated tGPH fluorescence overlaps with glia and immature neurons (arrows in C). (B, D) *repo>Pvr*^{RNAi} brains showed reduced tGPH membrane fluorescence in both glia and immature neurons (arrows in D) compared to wild-type.

Figure S13 Genotypes:
(A, C) *tGPH/+;repo-Gal4 UAS-tdTomato /+*
(B, D) *tGPH/UAS-Pvr*^{RNAi}*;repo-Gal4 UAS-tdTomato /+*

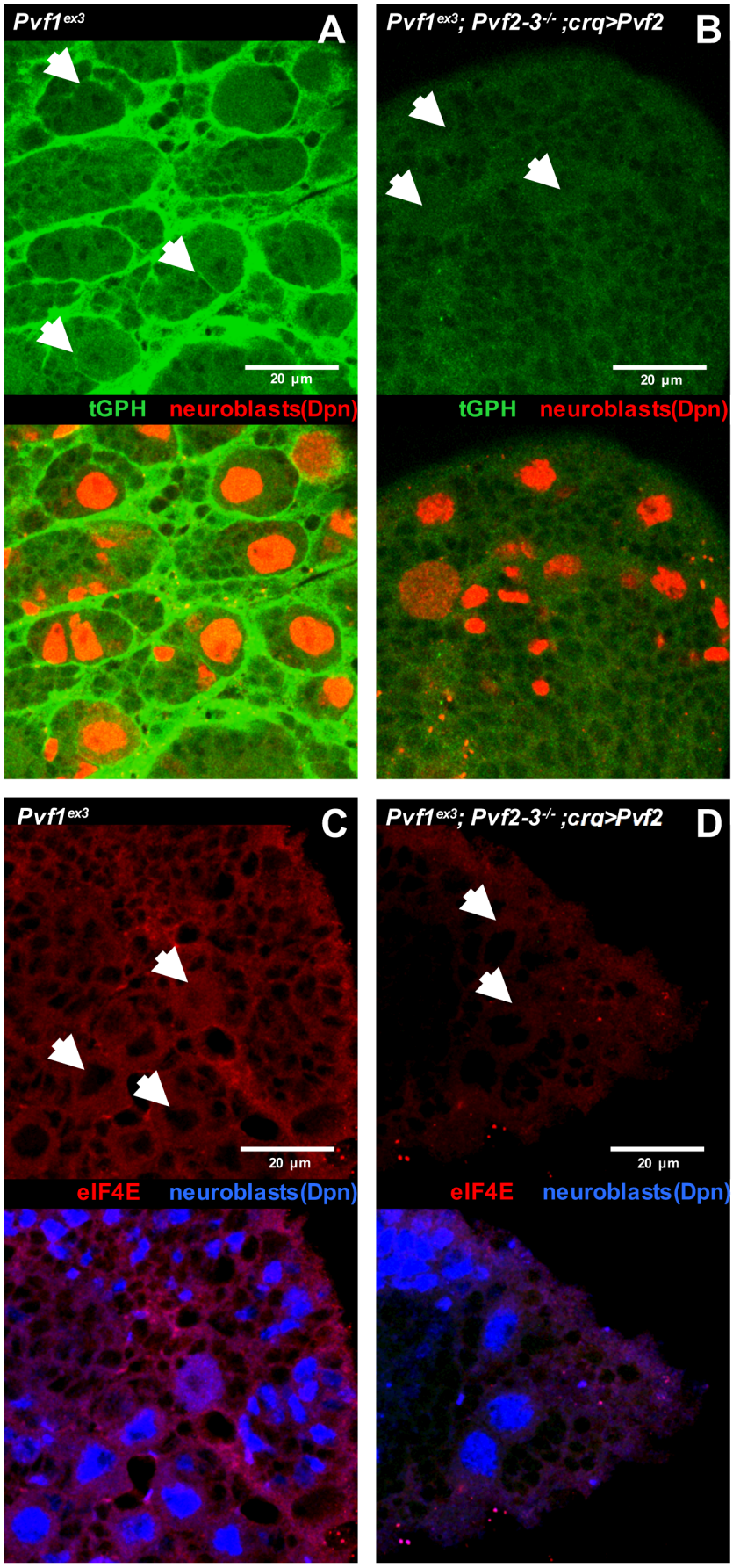

Figure S14: Loss of Pvf function causes cell autonomous and non-autonomous loss of PI3K

signaling

(A-B) Close-up views of 2 μm optical confocal sections from age-matched 3rd instar brains, all at the same scale. *Pvf1*^{ex3} (sibling control) and *Pvf1*^{ex3}; *Pvf2-3*$^{-/-}$ mutant brains harbor the tGPH PI3K reporter, which is a fusion between a plextrin homology domain and EGFP that localizes to the inner leaflet of the cell membrane in a PIP3-dependent manner. Dpn (red) labels neuroblasts. Glial membranes are not labeled by any *Gal4* driver. (A) Note that, in single *Pvf1*^{ex3}mutants, most membrane-associated tGPH membrane fluorescence appears to be glial, although tGPH membrane fluorescence is visible in Dpn+ neuroblasts (arrows). (B) *Pvf1*^{ex3}; *Pvf2-3*$^{-/-}$ mutant brains show reduced tGPH membrane fluorescence in both glia and neuroblasts (arrows), as compared to *Pvf1*^{ex3} single mutant or wild-type controls (see Figure 4 for wild-type).

(C, D) Close-up views of 2 μm optical sections from age-matched 3rd instar brains, all at the same scale. *Pvf1*^{ex3} (sibling control) and *Pvf1*^{ex3}; *Pvf2-3*$^{-/-}$ mutant brains stained for eIF4E protein (red), which, at high levels, indicates stable PI3K signaling (Song and Lu, 2011), and is known to be highly expressed in neuroblasts (Hsieh and Ruggero, 2010). Dpn (blue) labels neuroblasts. (D) *Pvf1*^{ex3}; *Pvf2-3*$^{-/-}$ mutant brains show over-all reduced eIF4E staining in all cell types, particularly in neuroblasts (arrows), as compared to *Pvf1*^{ex3} single mutants, which have a wild-type phenotype.

Figure S14 Genotypes:
(A) *Pvf1*^{ex3}*; +/CyO; tGPH/+* (sibling control for *Pvf1*^{ex3}*; Pvf2-3*$^{-/-}$ mutants)
(B) *Pvf1*^{ex3}*; Pvf2-3*$^{-}$ *crq-Gal4/Pvf2-3*$^{-}$ *UAS- Pvr*$^{\lambda}$*; tGPH/+*
(C) *Pvf1*^{ex3}*; +/CyO* (sibling control for *Pvf1*^{ex3}*; Pvf2-3*$^{-/-}$ mutants)
(D) *Pvf1*^{ex3}*; Pvf2-3*$^{-}$ *crq-Gal4/Pvf2-3*$^{-}$ *UAS- Pvr*$^{\lambda}$

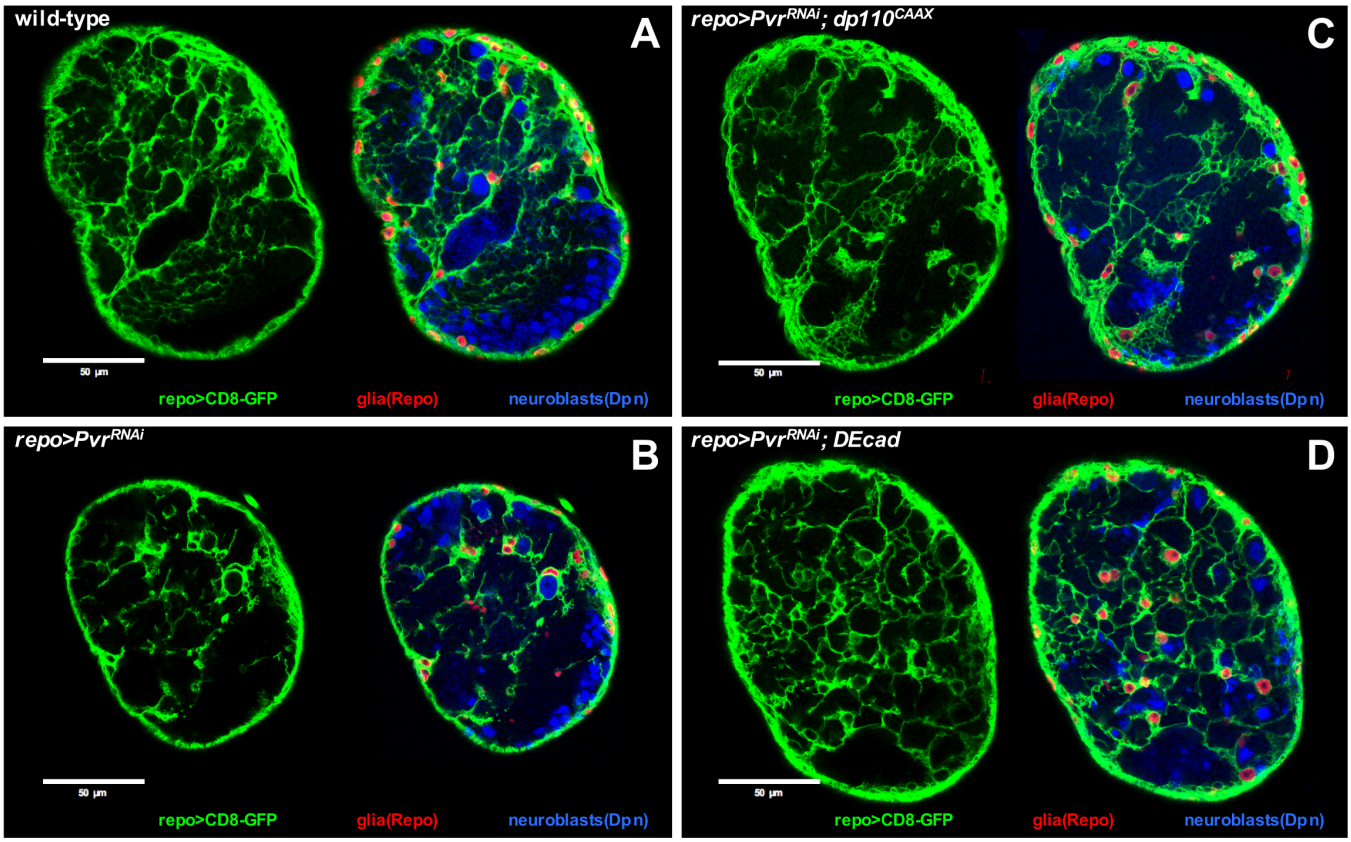

Figure S15: Loss of glial Pvr signaling is rescued by PI3K and DEcadherin signaling

(A-D) 2 µm optical sections of 3rd instar brain hemispheres, shown at similar section planes, at the same scale. *repo>CD8-GFP* labels glial cells; Dpn (blue) labels neuroblasts; Repo (red) labels glia. Note that the representative brain hemispheres of *repo>Pvr^{RNAi};dp110^{CAAX}* and *repo>Pvr^{RNAi};DEcad* animals showed phenotypes comparable to wild-type animals, with increased size, increased Dpn+ cells, and increased density of cortex glia and cortex glial cell projections compared to *repo>Pvr^{RNAi}* control animals.

Figure S15 Genotypes:
(A) *UAS-CD8-GFP/UAS-lacZ;repo-Gal4/+*
(B) *UAS-Pvr^{RNAi}/+;repo-Gal4 UAS-CD8-GFP/+*
(C) *UAS-dp110^{CAAX}/+; UAS-Pvr^{RNAi}/+;repo-Gal4 UAS-CD8-GFP/+*
(D) *UAS-Pvr^{RNAi}/UAS-DEcad;repo-Gal4 UAS-CD8-GFP/+*

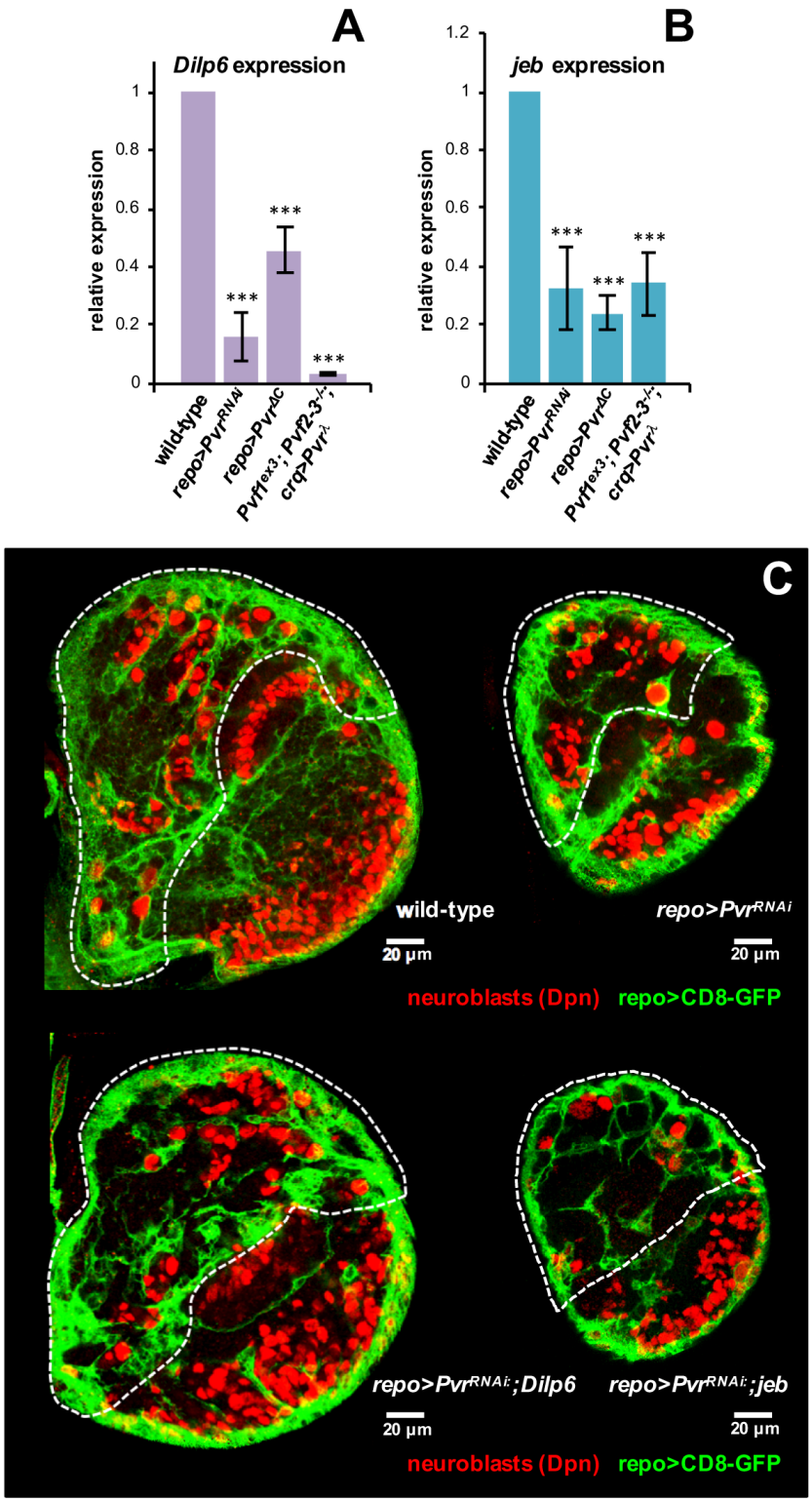

Figure S16: Loss of glial Pvr signaling is rescued by Dilp overexpression

(A-B) qPCR on RNA extracted from 3rd instar brain lobes. *Dilp3* and *Dilp6* expression calculated for each genotype relative to *gapdh* using the ΔΔCq method. *Dilp3*, *Dilp6*, and *jeb* expression in *repo>Pvr*^{RNAi}, *repo>Pvr*$^{\Delta C}$;*Pvr*$^{C02195/+}$, and *Pvf1*^{ex3};*Pvf2-3*$^{-/-}$*crq>Pvr*$^{\lambda}$ animals normalized to *Dilp3* and *Dilp6* in wild-type. Bars show confidence intervals for *Dilp3*, *Dilp6*, and *jeb* expression, calculated using normalized ΔΔCq values for 2-4 replicates each. Wild-type and mutants compared with a

student's two-tailed t-test. ***p-value <.005.

(C) 2 μm optical sections of 3rd instar brain hemispheres, at the same scale. *repo>CD8-GFP* labels glial cells; Dpn (red) labels neuroblasts. The central brain (dashed lines) in *repo>Pvr^{RNAi};Dilp6*, but not *repo>Pvr^{RNAi};jeb*, showed increased size and increased Dpn+ cells compared to *repo>Pvr^{RNAi}*.

Figure S16 Genotypes:
(A-B) *UAS-CD8-GFP;repo-Gal4/+*, *UAS-Pvr^{RNAi}/+;repo-Gal4 UAS-CD8-GFP/+*, *UAS-Pvr$^{\Delta C}$/Pvr^{C02195}; repo-Gal4 UAS-CD8-GFP/+*, *Pvf1^{ex3};Pvf2-3 crq-Gal4/Pvf2-3 UAS-Pvr$^{\lambda}$;UAS-CD8-GFP/+*
(C) *UAS-CD8-GFP;repo-Gal4/+*, *UAS-lacZ/UAS-Pvr^{RNAi};repo-Gal4 UAS-CD8-GFP/+* (UAS-lacZ controls for Gal4-UAS gene dose), *UAS-Dilp6/UAS-Pvr^{RNAi};repo-Gal4 UAS-CD8-GFP/+*, *UAS-jeb/UAS-Pvr^{RNAi};repo-Gal4 UAS-CD8-GFP/+*

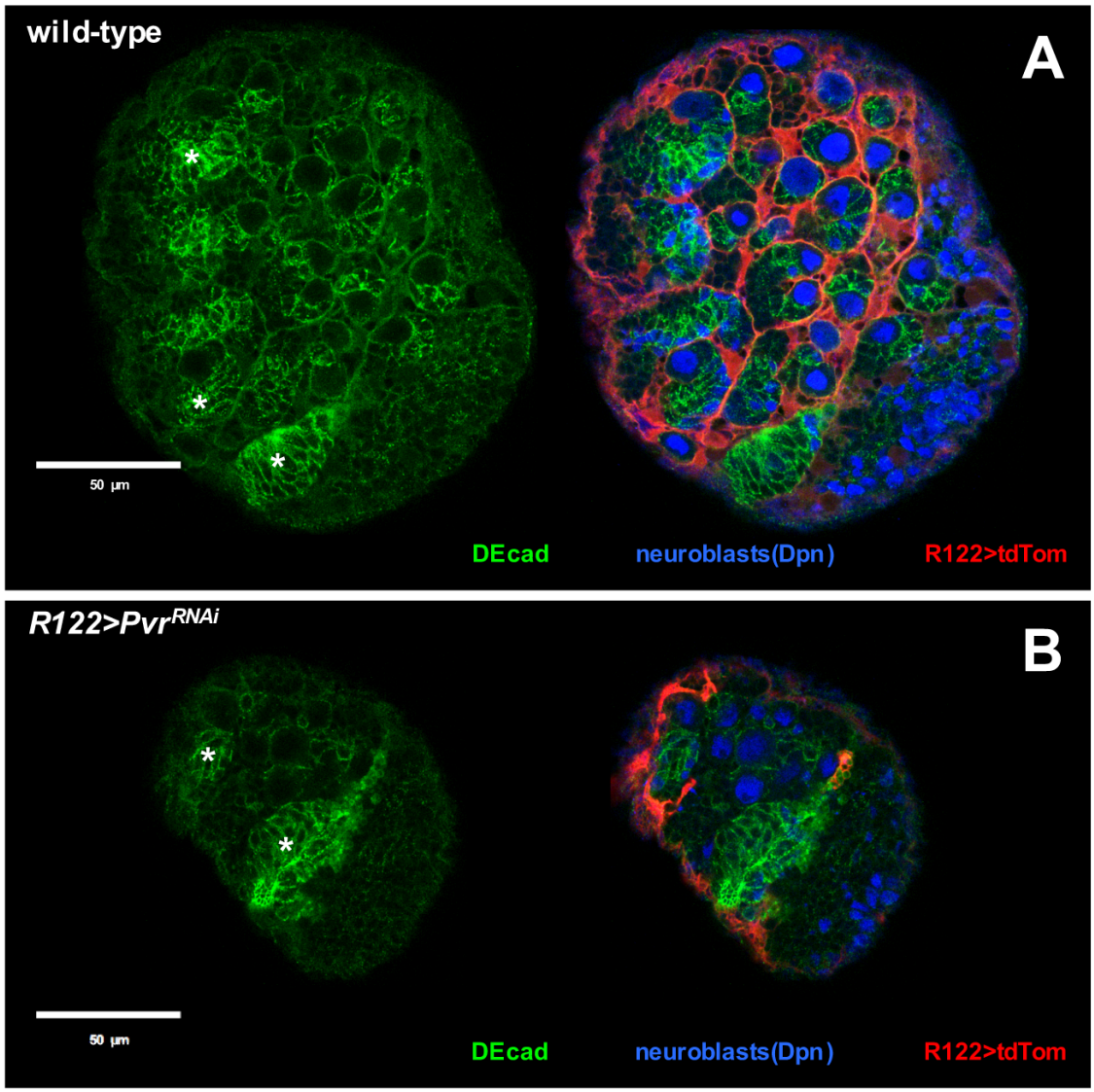

Figure S17: Loss of glial Pvr signaling causes loss of DE-cadherin localization

(A, B) 2 µm optical sections of age-matched 3rd instar brains, shown at similar section planes, at the same scale. Anterior up; midline to left. Green shows DEcad-GFP reporter localization; *R122>tdTom* (red) labels cortex glia membranes; Dpn (blue) labels neuroblast nuclei. (A) in wild-type, membrane-associated DEcad-GFP fluorescence overlaps with glia and neuroblast cell membranes (overlay) as well as immature neurons (asterisks). (B) *R122>Pvr^{RNAi}* showed reduced DEcad-GFP membrane fluorescence in both glia and neuroblasts (overlay) compared to wild-type, but retains DEcad-GFP expression in immature neurons (asterisks).

Figure S17 Genotypes:
(A) *shg-DEcadGFP/+;R122-Gal4 UAS-tdTomato/+*
(B) *shg-DEcadGFP/UAS-Pvr^{RNAi};R122-Gal4 UAS-tdTomato/+*

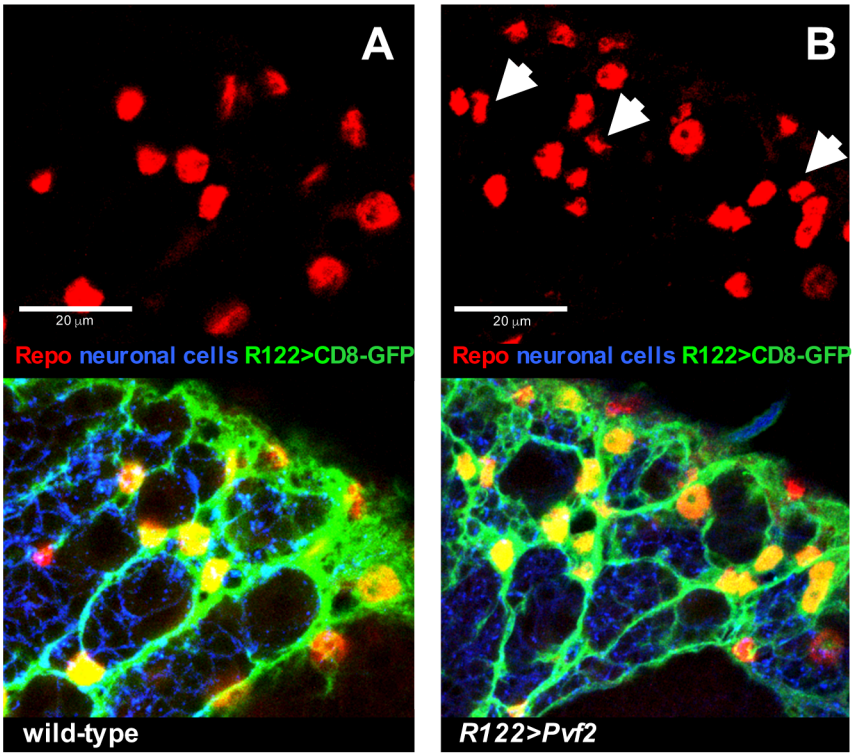

Figure S18: Pvf overexpression causes accumulation of excess cortex glia

(A, B) Close-up views of 2 µm optical sections of age-matched 3rd instar brains, all at the same scale. Anterior up; midline to left. Cortex glia cell bodies and processes are labeled with membrane-associated tdTomato driven by *R122-Gal4* (tdTom, false colored green); Repo (red) labels glial cell nuclei; HRP stain (blue) labels neuroblast and neuronal cell bodies. (B) *R122>Pvf2* mutants show an increased number of dtTom-Repo-positive cortex glia in the central brain (arrows, upper panel) as compared to (A) wild-type.

Figure S18 Genotypes:
(A) *R122-Gal4 UAS-tdTomato/+*
(B) *UAS-Pvf2/+; R122-Gal4 UAS-tdTomato/+*

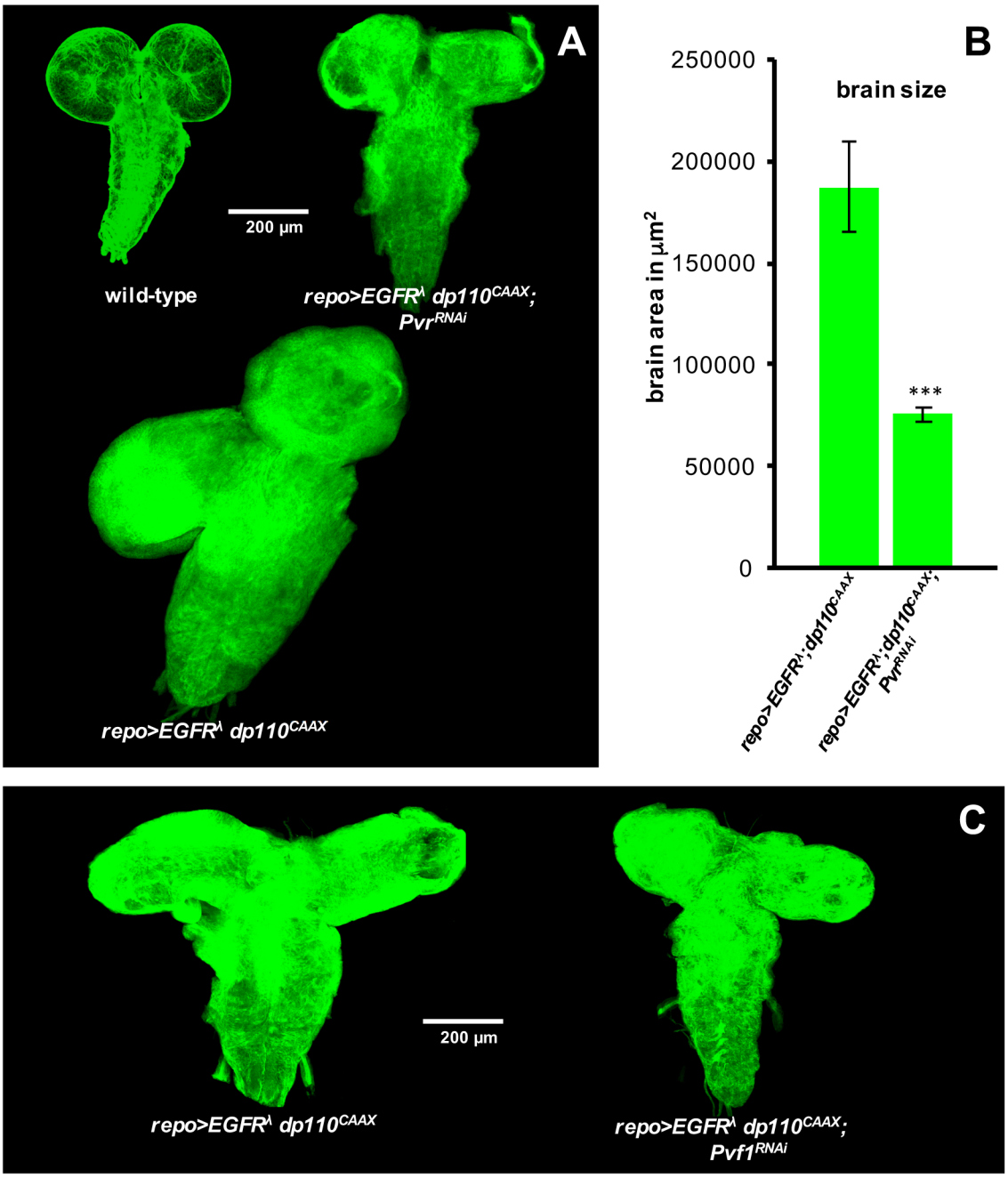

Figure S19: Pvr signaling drives glial neoplasia

(A) Optical projections of late 3rd instar larval brains, approximately 130 hr AED, all at the same scale. Dorsal view; anterior up. *repo>CD8-GFP* (green) labels glial cell bodies. A dramatic increase in over-all larval brain size is caused by neoplastic transformation of glia by constitutively active EGFR and PI3K signaling (*repo>dEGFR$^{\lambda}$;dp110^{CAAX}*) (Read et al., 2009), as compared to wild-type. EGFR-dependent neoplastic glial overgrowth is dramatically reduced upon knockdown of *Pvr* (*repo>dEGFR$^{\lambda}$;dp110^{CAAX};Pvr^{RNAi}*).

(B) The effects of *Pvr* knockdown on brain size in *repo>dEGFR$^{\lambda}$;dp110^{CAAX}*. Brain size calculated using total brain area, measured in µm^2 in optical projections of late 3rd instar brains. This showed that *repo>dEGFR$^{\lambda}$;dp110^{CAAX};Pvr^{RNAi}* (n=3) mutants are significantly smaller than

repo>dEGFR$^{\lambda}$;dp110^{CAAX} (n=3), as determined with pair-wise comparison using a student's two-tailed t-test. ****p-value* <.005. Error bars indicate standard error of the mean.

(C) Optical projections of late 3rd instar larval brains, approximately 130 hr AED, all at the same scale. Dorsal view; anterior up. *repo>CD8-GFP* (green) labels glial cell bodies. EGFR-dependent neoplastic glial overgrowth is partially reduced upon knockdown of *Pvf1* (*repo>dEGFR$^{\lambda}$;dp110^{CAAX};Pvf1^{RNAi}*).

Figure S19 Genotypes:

(A-B) *UAS-CD8-GFP/+;repo-Gal4/+* , *UAS-dEGFR$^{\lambda}$ UAS-dp110^{CAAX}/+;repo-Gal4 UAS-CD8-GFP/+* , *UAS-dEGFR$^{\lambda}$ UAS-dp110^{CAAX}/+;UAS-Pvr^{RNAi}/+;repo-Gal4 UAS-CD8-GFP/+*

(C) *UAS-dEGFR$^{\lambda}$ UAS-dp110^{CAAX}/+;repo-Gal4 UAS-CD8-GFP/+* , *UAS-dEGFR$^{\lambda}$ UAS-dp110^{CAAX}/+; UAS-Pvf1^{RNAi}/repo-Gal4 UAS-CD8-GFP*

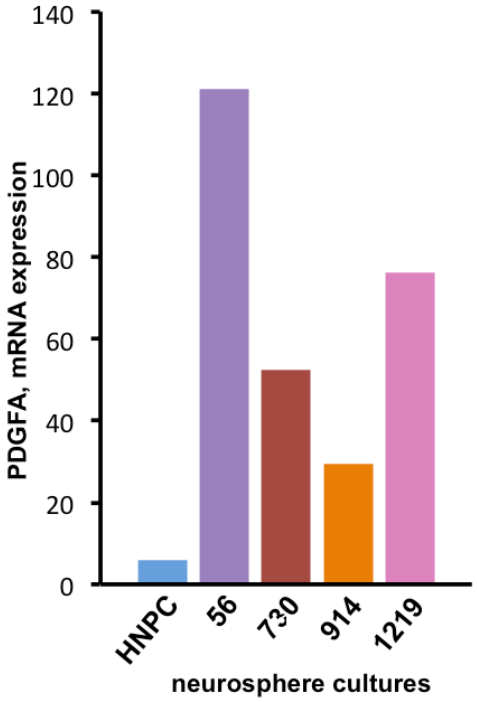

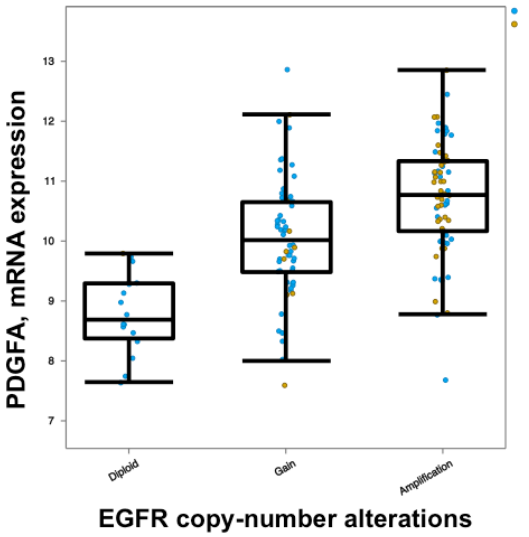

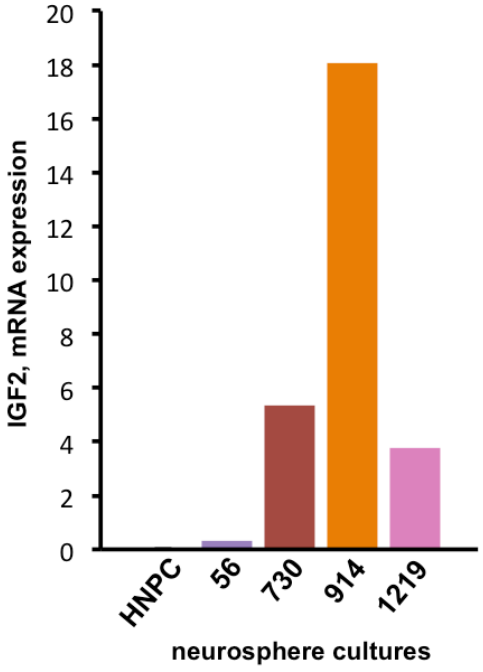

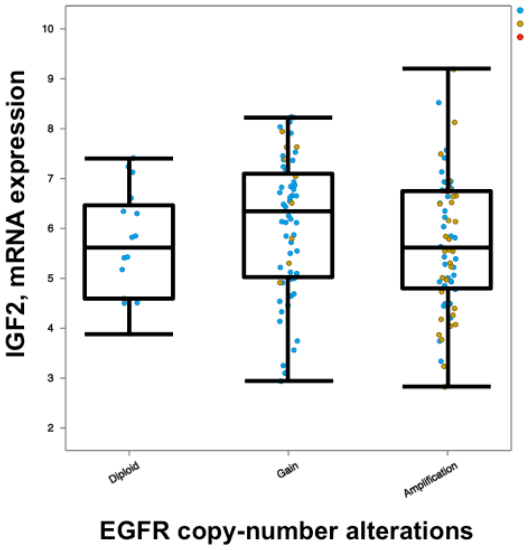

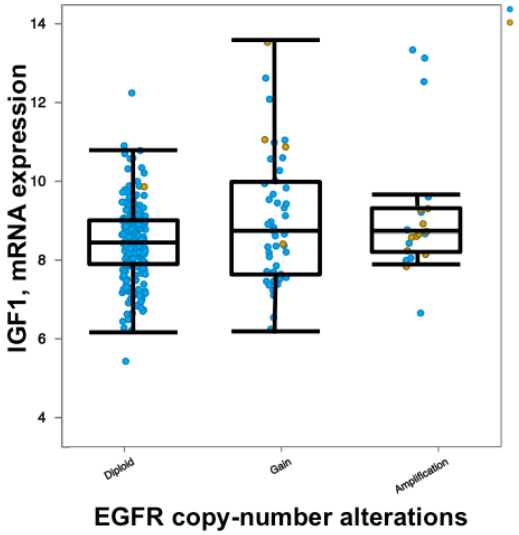

Figure S20: PDGFA, IGF1, IGF2 expression in human glioblastomas in association with RTK alterations

(A,B) Graphs show normalized mRNA expression levels for (A) PDGFA or (B) IGF2 in primary neurosphere stem cell cultures of normal human neural progenitor cells (HNPCs) and human glioblastoma (GBM) cells that harbor RTK alterations in MET (56, 730, 914) and/or EGFR (914, 1219). mRNA expression levels obtained from RNAseq profiling of each indicated primary cell culture.

(C) Table shows tendency towards co-occurrence of alterations in gene expression, coding sequence, copy number, or mRNA expression levels in GBM for the indicated loci. Values obtained from TCGA datasets for GBM through the cBio Portal (www.cbioportal.org) (Brennan et al., 2013; Cancer Genome Atlas Research et al., 2015).

(D-F) Graphs show mRNA expression levels for (D) PDGFA, (E) IGF2, or (F) IGF1 plotted relative to EGFR copy number alterations in primary human (D, E) GBM tumor tissue or (F) lower grade glioma tumor tissue (grade II and III gliomas). Blue indicates tumors with no mutations in either locus; orange indicates tumors with mutations in one locus; red indicates tumors with mutations in both loci. Values obtained from TCGA datasets for GBM and low grade gliomas through the cBio Portal (www.cbioportal.org) (Brennan et al., 2013; Cancer Genome Atlas Research et al., 2015).

References

Avet-Rochex, A., Kaul, A.K., Gatt, A.P., McNeill, H., and Bateman, J.M. (2012). Concerted control of gliogenesis by InR/TOR and FGF signalling in the Drosophila post-embryonic brain. Development *139*, 2763-2772.
Awasaki, T., Lai, S.L., Ito, K., and Lee, T. (2008). Organization and postembryonic development of glial cells in the adult central brain of Drosophila. J Neurosci *28*, 13742-13753.
Brennan, C.W., Verhaak, R.G.W., McKenna, A., Campos, B., Noushmehr, H., Salama, S.R., Siyuan Zheng, S., Chakravarty, D., Sanborn, J.Z., Berman, S.H., *et al.* (2013). The Somatic Genomic Landscape of Glioblastoma. Cell *155*, 462-477.
Cancer Genome Atlas Research, N., Brat, D.J., Verhaak, R.G., Aldape, K.D., Yung, W.K., Salama, S.R., Cooper, L.A., Rheinbay, E., Miller, C.R., Vitucci, M., *et al.* (2015). Comprehensive, Integrative Genomic Analysis of Diffuse Lower-Grade Gliomas. N Engl J Med *372*, 2481-2498.
Castilho, B.A., Shanmugam, R., Silva, R.C., Ramesh, R., Himme, B.M., and Sattlegger, E. (2014). Keeping the eIF2 alpha kinase Gcn2 in check. Biochim Biophys Acta *1843*, 1948-1968.
Ghillebert, R., Swinnen, E., Wen, J., Vandesteene, L., Ramon, M., Norga, K., Rolland, F., and Winderickx, J. (2011). The AMPK/SNF1/SnRK1 fuel gauge and energy regulator: structure, function and regulation. The FEBS journal *278*, 3978-3990.
Hsieh, A.C., and Ruggero, D. (2010). Targeting eukaryotic translation initiation factor 4E (eIF4E) in cancer. Clin Cancer Res *16*, 4914-4920.
Metaxakis, A., Oehler, S., Klinakis, A., and Savakis, C. (2005). Minos as a genetic and genomic tool in Drosophila melanogaster. Genetics *171*, 571-581.
Nakano, I., and Kornblum, H.I. (2009). Methods for analysis of brain tumor stem cell and neural stem cell self-renewal. Methods Mol Biol *568*, 37-56.
Poon, C.L., Lin, J.I., Zhang, X., and Harvey, K.F. (2011). The sterile 20-like kinase Tao-1 controls tissue growth by regulating the Salvador-Warts-Hippo pathway. Dev Cell *21*, 896-906.
Read, R.D., Cavenee, W.K., Furnari, F.B., and Thomas, J.B. (2009). A drosophila model for EGFR-Ras and PI3K-dependent human glioma. PLoS Genet *5*, e1000374.
Read, R.D., Fenton, T.R., Gomez, G.G., Wykosky, J., Vandenberg, S.R., Babic, I., Iwanami, A., Yang, H., Cavenee, W.K., Mischel, P.S., *et al.* (2013). A kinome-wide RNAi screen in Drosophila Glia reveals that the RIO kinases mediate cell proliferation and survival through TORC2-Akt signaling in glioblastoma. PLoS Genet *9*, e1003253.
Song, Y., and Lu, B. (2011). Regulation of cell growth by Notch signaling and its differential requirement in normal vs. tumor-forming stem cells in Drosophila. Genes Dev *25*, 2644-2658.
Speder, P., and Brand, A.H. (2018). Systemic and local cues drive neural stem cell niche remodelling during neurogenesis in Drosophila. eLife *7*.
Trapnell, C., Roberts, A., Goff, L., Pertea, G., Kim, D., Kelley, D.R., Pimentel, H., Salzberg, S.L., Rinn, J.L., and Pachter, L. (2012). Differential gene and transcript expression analysis of RNA-seq experiments with TopHat and Cufflinks. Nat Protoc *7*, 562-578.
Van Aelst, L., and Symons, M. (2002). Role of Rho family GTPases in epithelial morphogenesis. Genes Dev *16*, 1032-1054.